

DETAILED TECHNICAL REPORT

"APPLICATION OF REMOTE SENSING FOR
PREDICTION AND DETECTION OF THERMAL POLLUTION"

Reproduced by
NATIONAL TECHNICAL
INFORMATION SERVICE
US Department of Commerce
Springfield, VA. 22151

by

T. Nejat Veziroglu and Samuel S. Lee

prepared for

NATIONAL AERONAUTICS AND SPACE ADMINISTRATION

NASA CONTRACT NAS10 - 8498



Clean Energy Research Institute

School of Engineering and Environmental Design

University of Miami

Coral Gables, Florida

October, 1974

(NASA-CR-139182) APPLICATION OF REMOTE
SENSING FOR PREDICTION AND DETECTION OF
THERMAL POLLUTION (Miami Univ.) 100 P
HC \$4.75 CSCL 13B
G3/43 53700 Unclas

STANDARD TITLE PAGE			
1. Report No. CR - 139182		2. Government Accession No.	
4. Title and Subtitle Application of Remote Sensing for Prediction and Detection of Thermal Pollution		3. Recipient's Catalog No.	
7. Author(s) T. Nejat Veziroglu and Samuel S. Lee		5. Report Date October, 1974	
9. Performing Organization Name and Address Clean Energy Research Institute School of Engineering and Environmental Design, University of Miami Coral Gables, Florida, 33124		6. Performing Organization Code	
12. Sponsoring Agency Name and Address John F. Kennedy Space Center Kennedy Space Center, Florida		8. Performing Organization Report No.	
10. Work Unit No.		11. Contract or Grant No. NAS 10-8498	
13. Type of Report and Period Covered Detailed Technical Report		14. Sponsoring Agency Code	
15. Supplementary Notes PRICES SUBJECT TO CHANGE			
16. Abstract Thermal Pollution has been identified as one of the important problems to be considered in a <u>NASA Environmental Quality Enhancement Program Study</u> . Proper management of this problem will be based on the ability to detect thermal pollution and to alleviate it. Also, in order to obtain a clear description of the physical situation, an accurate prediction of the water body temperature distribution is needed. This report covers the first phase of a three year project aimed at the development of a predictive mathematical model for thermal pollution in connection with remote sensing measurements. This study has several objectives: 1) The development and testing of a generalized mathematical model to predict three-dimensional temperature distribution in coastal regions receiving hot discharges; 2) the improvement in the accuracy of the thermal remote sensing by directly relating it to thermal radiation from the sea surface and by better accounting for the absorption in the atmosphere; and 3) the development and testing of an active remote sensing system to measure the water turbidity. In the model development, a rigid-lid model has been developed and results have been obtained for different wind conditions. The next step is to include tidal effects. Biscayne Bay in So. Fla., the site of two Fla. Power Plant facilities, is being used for model testing. In the experimental part, the design of the measurement system has been completed. Necessary instruments needed for the first stage of experiment has been acquired, tested and calibrated. A preliminary research flight of the Kennedy Space Center NASA-6 Beechcraft, in cooperation with satellite thermal I.R. radiometer and ground truth data collection by boat, was carried out on July 29, 1974.			
17. KeyWords Thermal Pollution, Remote Sensing Mathematical Model <i>na</i>		18. Distribution Statement Unlimited - STAR	
19. Security Classif.(of this report) Unclassified	20. Security Classif.(of this page) Unclassified	21. No. of Pages	22. Price

Detailed Technical Report

Application of Remote Sensing for Prediction
and Detection of Thermal Pollution

by

T. Nejat Veziroglu & Samuel S. Lee

Prepared for:

National Aeronautics and Space Administration
(NASA Contract NAS10-8498)

Clean Energy Research Institute
School of Engineering and Environmental Design

University of Miami
Coral Gables, Florida

October 8, 1974

14

University of Miami
Clean Energy Research Institute
Thermal Pollution Research Team

Principal Investigators:

Dr. T. Nejat Veziroglu
Director, Clean Energy Research Institute

Dr. Samuel S. Lee
Director, Thermal Pollution Research Laboratory

Investigators:

Dr. Homer Hiser
Director, Remote Sensing Laboratory

Dr. Norman Weinberg
Professor of Electrical Engineering

Dr. Joseph Hirschberg
Director, Optics Laboratory

Dr. Subrata Sengupta
Research Associate

Research Assistants:

James Byrne

Jeffrey McGrath

Ching-Fen Tsai

Tyag R. Sehgal

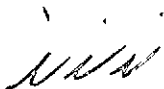
A handwritten signature, possibly reading "N. V.", is located at the bottom center of the page.

TABLE OF CONTENTS

	Page
I. <u>Introduction</u>	1
II. <u>Mathematical Model</u>	8
A. Introduction	
B. The Far Field	
C. The Near Field	
D. Some Rigid-Lid Results	
III. <u>Ground Truth and In-Situ Measurements</u>	59
A. Objective	
B. Measurements System	
C. Procedures	
D. Results and Discussion	
IV. <u>Remote Sensing Water Surface Temperature</u>	79
A. Air Force Satellite Data	
B. NOAA Satellite Data	
C. NASA-6 Aircraft Flight	
D. Radisonde Data for Water Vapor Corrections of IR Measurements	
E. Satellite Data and Results	



I. INTRODUCTION

Many industrial plants, especially electric power generating plants, use large quantities of water for cooling purposes. When heated waters from such industrial plants are discharged into rivers, lakes and estuaries, they can disturb the ecological balance and destroy the natural habitat of aquatic life by changing the temperature levels. In rivers the hot discharge waters can cause miles of hot sections which act as thermal barriers and prevent fish from going upstream to their spawning grounds. In regions of high ambient temperatures, such as along the East Coast of Florida, the hot discharges can cause excessive estuarine temperatures. This in turn increases the evaporation and results in an overall increase in the level of salinity. Turbidity of mineral origin can be generated by the dislodging and suspension of sediments by currents such as those caused by hot discharges. Turbidity of biological origin can be generated by photoplankton growth in thermally suitable environments. The above outlined processes can ruin the marine environment as far as ecological, fishing and recreational interests are concerned.

A major source of thermal pollution of rivers, lakes and estuaries is the hot water discharge from the condensers of fossil and nuclear fueled power plants. The demand for electric power in the world is now doubling every nine years, and indications are that the rate of increase will be even greater in the coming decades. About 5500 BTU of thermal energy are produced for every kilowatt hour of electricity generated by a conventional power plant. Nuclear powered plants, being less efficient, produce about 10,000 BTU per kilowatt hour. This means that the doubling time for hot discharges, the cause of thermal pollution, is less than nine years, or about eight years.

In order to meet the growing cooling water requirements, it is projected that by 1980, thirty-two percent of all steam electric stations will be located adjacent to estuaries or on open sea coasts. The problems associated with the release of these large

volumes of heated water are compounded by recent trends within the power industry. Large plants, including more nuclear powered generators, are being built, and groups of these units will be located at a single site. Thus the United States, and the world, face a potential problem in environmental alteration of enormous proportions, particularly in estuarine and coastal marine waters.

In a report ¹ on Potential NASA Initiative in Water Resources, it is pointed out that controlling the heated water discharges has been identified by the Office of Water Resources Research as one of the important problem areas. Thermal pollution is also one of the problems to be considered in a NASA Environmental Quality Enhancement Program Study ². Proper management will be based on the ability to detect thermal pollution and to alleviate it. In order to achieve this goal, it is necessary to have a thorough understanding of the motion and diffusion of thermal discharges and the extent of the region affected. Most studies in this area have been empirical or semi-empirical in nature. The few existing models are based on much too simplified assumptions and are limited to one or two-dimensional studies. In order to obtain a better description of the physical situation, a more accurate prediction of the water body temperature distribution is needed.

In a NASA sponsored feasibility study completed in January 1974, a team of researchers at the University of Miami concluded that it is feasible to develop a generalized three-dimensional predictive, mathematical model, involving remote sensing and in situ measurements to supply necessary parameters. It was recommended that the development of the mathematical model be conducted over four phases covering a time period of three years. Three sites were proposed to be used for the development and testing of the model and for the development of remote sensing for thermal pollution and turbidity detection. These three power plant sites are the Florida Power and Light Company Turkey Point and

Cutler Ridge facilities and Port St. Lucie Nuclear Power Plant units on Hutchinson Island. These three sites are located in south Florida, close to both the Kennedy Space Center and the University of Miami. Another interesting feature is their geographical contrast. The Turkey Point and Cutler Ridge facilities are located at a shallow lagoon type estuary, while the Hutchinson plant discharges into the off-shore continental shelf. Both sites should provide a good test area for the universal nature of the proposed three-dimensional model.

The present contract, which was initiated in March, 1974 and covers a period of six months, covers the first phase of the model development. This study will serve the following purposes: (1) the development and testing of a generalized mathematical model to predict three-dimensional temperature and salinity distribution in coastal regions receiving hot discharges; (2) the improvement in the accuracy of the thermal remote sensing system by directly relating them to thermal radiation from the sea surfaces and by better accounting for the absorption in the atmosphere, and (3) the development and testing of an active remote sensing system to measure the water turbidity. This study program is being carried out in four parts. They are closely related and are to be conducted concurrently. The mathematical model development is the major part of the project. Remote sensing and in-situ measurements, the second and third parts, are needed to support the model development. At the same time, a turbidity remote sensing system is being developed. The relationship between these various phases of the study may be shown by a flow diagram in Fig. 1-1.

In the mathematical model development, the study has been divided into four tractable parts, whose results are to be synthesized for the overall model as follows: (1) a one-dimensional study of the energy equation with no horizontal transport, or

convective terms is being made. The results will be compared with field data. Conclusions regarding the magnitude and variation of the vertical eddy diffusivity can be made from this study. The solar radiation boundary condition and the form of the source term in the energy equation should also be available from this study; (2) a rigid-lid model for the Bay with no tidal effects will be used to give a reasonably clear picture of the wind-driven circulation in the Bay; (3) a free surface model including tidal boundary conditions will be the final general circulation model. The velocity and temperature fields obtained from this will be used as the far-field solution for the thermal discharge model; (4) the jet-discharge will be modeled with a horizontal stretching as well as a vertical one to transform the basin to a constant depth - one with the horizontal domain extending from $+1$ to -1 and 0 to $+1$, in the transverse and longitudinal directions, respectively. The combined results of (3) and (4) will constitute the predictions regarding thermal pollution in Biscayne Bay. The programs will be of sufficient generality to be applied to other basins with thermal discharges.

In this six month period, the rigid-lid model has been developed and results obtained for different wind conditions. The computer program is well behaved numerically for the closed basin approximation of Biscayne Bay. The next step is to include tidal effects. Finally, temperature will be included in the rigid-lid model. The one-dimensional study program is at an advanced stage. The computer program is ready and results are being compared with field data. More comparisons will be made as new data is collected for this project. The near-field problems have been formulated. Both free-surface and rigid-lid formulations have been done. The programming has been initiated. The free surface far-field formulation and programming has been completed. Debugging and modifications will be initiated soon.

The experimental part of this project serves many purposes. It is to provide ground truth for remote sensing measurements, to provide initial and boundary conditions and verification of the mathematical model, and to assist in the development of new remote sensing techniques. This part of the study can be divided into three related experiments, namely; 1) Ground Truth and In-Situ Measurements, 2) Remote Sensing Water Surface Temperature Study, and 3) Turbidity Laser System and Ground Truth Water Surface Temperature Study. In this first phase of the program, the design of the measurement system has been completed. Necessary instruments needed for the first stage of the experiment have been acquired, tested and calibrated. Test runs have been carried out in Biscayne Bay to establish proper procedures for shipboard measurements. For the remote sensing experiment, radiosonde data in Miami area has been collected for water vapor corrections of infra-red Measurements. Arrangements have been made to obtain I.R. data from the Air Force Defense Meteorological Satellite Program (DMSP), formerly DAPP, Satellites and the National Oceanic and Atmospheric Administration NOAA-2 and NOAA-3, IIOS Series of Satellites. On July 29, 1974, the Kennedy Space Center NASA-6 Beechcraft C-45H made research flights over Biscayne Bay at Miami, Florida, while NOAA and Air Force Satellites with thermal IR radiometers were passing overhead and a boat was gathering ground truth data in the bay. The aircraft flew at 1500 ft. altitude and made twelve west to east data passes across Biscayne Bay between 0800 EDT (1200 Z) and 1300 EDT (1700 Z). This experimental data has been analysed and certain problem areas have been corrected. It is felt that these preliminary experiments have achieved its goals. Procedures have been established, and all personnel have been trained in the operation of all the instruments. From the trial runs and the experience acquired in the use of the instruments and handling of remote sensing data, the team is ready to conduct further experiments in the latter part of the program.

Detailed reports on the various parts of the present study are given in the following chapters.

References

1. Tremor, J.W., "Potential NASA Initiative in Water Resources", NASA Office of Applications, 1974.
2. NASA Office of Applications, "Environmental Quality Enhancement Program Study", 1972.

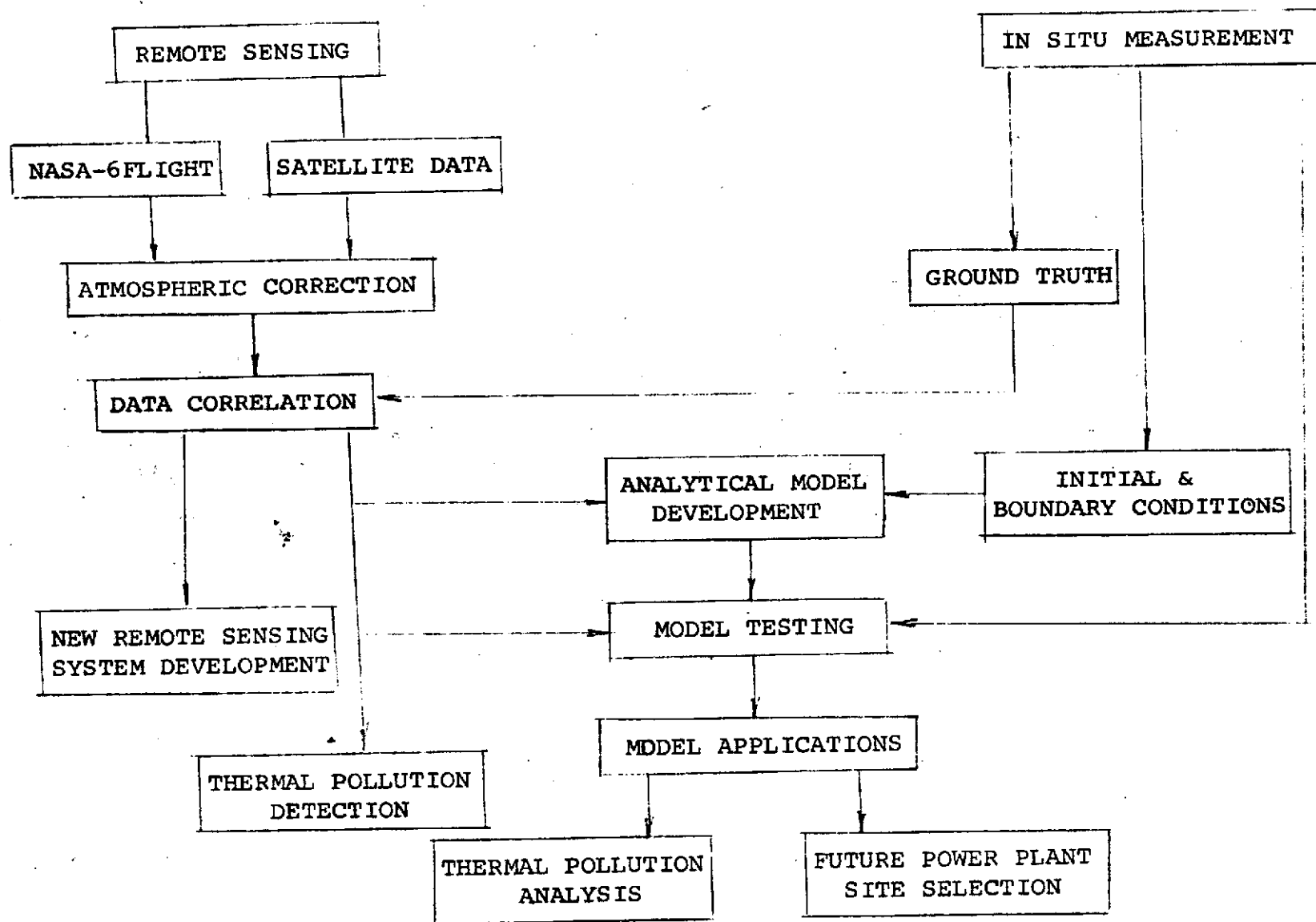


Fig. 1-1. Relationships between various phases of the program.

II. MATHEMATICAL MODEL

A. Introduction

1. The Need for Numerical Modeling

There has been a growing interest recently in the effects of chemical and thermal pollution on the environment. The effects can be directly harmful to the higher consumers in the food chain, e.g., fishes, man. More often, thermal pollution first affects the lower forms of life such as algae, plankton, and small organisms. Disturbances in the food chain propagate and the effects soon become apparent. Sometimes entire species of plankton or algae vanish from the ecosystem. In rivers the hot discharges can cause miles of hot sections which act as thermal barriers and prevent fish from going upstream to their spawning grounds. In regions of high ambient temperatures, such as along the east coast of Florida, the hot discharges can cause excessive estuarine temperatures. This increases the evaporation and results in an overall increase in the level of salinity. Turbidity of mineral origin can be generated by the dislodging and suspension of sediments by currents such as those caused by hot discharges. Turbidity of biological origin can be generated by phytoplankton growth in thermally suitable environments. The above outlined processes can ruin the marine environment as far as ecological, fishing and recreational interests are concerned. A more serious effect sometimes is the distortion of coastal aquifers used for water supply.

The sources of pollution usually are sewage systems, power plant cooling systems (open cycle), industrial discharge into lakes and rivers, and other installations which use the environment as a direct chemical or thermal sink.

For a meaningful study of the effects of pollution on the chemistry, biology, or zoology of an ecosystem, it is imperative that the hydrodynamic and thermodynamic information may be used in the overall ecological model.

One of the major problems in experimental modeling of large ecosystems like Biscayne Bay is the difficulty of reproducing the turbulent scales in laboratory facilities. The eddy viscosities vary by orders of magnitude. Consequently, there is always the possibility of getting observations from laboratory facilities which do not model flows on geophysical scales, even qualitatively.

This indicates the necessity of numerical modeling. A numerical model may be used to simulate various limiting situations with relative ease. Besides, decisions can be made a priori regarding the environmental impact of facility locations. Numerical modeling is therefore an invaluable tool for making decisions regarding siting of power plants.

2. Biscayne Bay

Fig. 2.1 shows a map of the Biscayne Bay area. The numerical model must incorporate the general, wind-driven and tide-driven circulation in the Bay together with the velocity and temperature field distortions caused by thermal discharges. The Bay is about 25 kilometers long and 8 kilometers wide in its maximum reaches. The Bay has several basins connected by shallow limestone sills. The major flow into the Bay comes through the shoal areas located at the northeastern part of Biscayne Bay. This is about 16 kilometers in length, with the shallow limestone sills varying from 1 to 3 kilometers in width. The mean low water is from 1 to 3 ft. in depth, with about 20 channels with maximum depth up to 15 ft. There are several other inlets at Bear Cut and lower Biscayne Bay connecting it to the Atlantic Ocean. Broad Creek, Angelfish Creek, and Caesar Creek are the significant connecting channels.

The main basin is divided in the middle by Feather Bed Bank. Cutler Bank and Card Bank demarcate the other two basins, namely Card Sound and Barnes Sound. The maximum depth of the Bay is around 12 ft.

3. Relevant Literature Survey

The numerical modeling effort may be divided into two separate studies. The first one comprises the general circulation and temperature field in the bay, under the action of tides, wind and solar heating. The second comprises the modeling of a buoyant heated jet with the general circulation model supplying some of the boundary and initial conditions. Therefore, the literature survey will first discuss the general circulation models and then the existing literature on modeling of thermal plumes.

Ekman [1]*was one of the earliest to investigate wind-driven circulation. Welander [2] modeled the time-dependent and steady-state solutions for the finite depth case. He found that the local time-histories of wind-stress and surface slope may be used to express the velocity and flow fields. He also found the sea level elevation in terms of a single integro-differential equation. He neglected the horizontal viscous terms and non-linear inertia terms in the Navier-Stokes equation.

Though these analytical models were adequate for understanding some of the basic characteristics of wind-driven circulation, numerical modeling became necessary for cases including effects of bottom topography, non-linear inertia terms and side-wall boundary layers.

Integrated stream-function models have been used by Gedney and Lick [3] and others for lake and ocean flows. These essentially are two-dimensional.

Numerical models of greater complexity have been developed by Bryan [4], Crowley [5,6,7], Berdahl [8] and others at Lawrence Radiation Laboratory. Bryan's and Crowley's models dealt with constant depth situations, for rectangular and irregular domains.

*Numbers in square brackets indicate references at end of report.

The major findings were that the rigid-lid model where vertical velocities are zero at the surface was adequate for the general circulation aspect but erroneous in predicting the Rossby wave speeds. The rigid-lid models were computationally superior in saving computer time. Berdahl [11] used the primitive equations of motion, rather than the stream function approach, e.g., Bryan [4]. He used a rigid-lid model and found the same advantages and disadvantages for the rigid-lid model in comparison to the free-surface model.

Sengupta and Lick [9] developed a rigid-lid model. They used a predictive equation for pressure derived from the horizontal momentum equation. The solution was advanced in time using explicit schemes on the momentum and energy equations. They avoided programming difficulties of a variable depth basin by a vertical stretching which converts it to a constant depth basin. This stretching was first suggested by Phillips [10] and later used by Freeman et al [11] in a free-surface model for Lake Huron.

Modeling of Biscayne Bay till now has been confined to two-dimensional considerations. Dean et al [12] used vertically integrated momentum equations to predict water elevations and discharges of the Biscayne Bay Card Sound system. They incorporated tidal effects and approximated the effects of shallow sills by using friction factors.

Extensive work has been done in the past few years on modeling thermal discharges from electric generating plants. A critical appraisal of the various existing models has been made by a team at Argonne National Laboratory. Reports by Policastro and Tokar [13], Policastro [14] and Policastro and Paddock [15] summarize these evaluations. The authors compared the models with field data from existing thermal discharges. The bulk of the models were two-dimensional with only a few considering the effects of buoyancy.

Paul and Lick [16] modeled the Cuyohoga River discharging into Lake Erie. Their model was three-dimensional in character, and effects of buoyancy were clearly illustrated. Waldrop and Farmer [17] modeled the discharge of a river into a crossflow. They excluded the effects of temperature gradient but included buoyancy effects due to salinity gradients. The applied transformation in the horizontal plane which mapped the semi-infinite domain into -1 to $+1$ and 0 to $+1$ in transverse and longitudinal direction to the river. This also resulted in grid structure which was constant in the transformed plane but increased in size away from the origin in the real plane. This allowed them to consider a large plane without too many grid points yet retaining fairly good resolution near the river mouth.

Rooth and Lee [18] have made a simple heat budget model for estimating steady state thermal anomaly areas from hot discharges. They ignored vertical structure of the flow mixing. Surface evaporation and sensible heat transfer at the surface were assumed to be the dominant heat transfer mechanisms.

4. General Considerations for the Present Investigation

A survey of recent literature indicates that it is numerically cumbersome to model the Biscayne Bay together with the thermal discharges simultaneously. The stability limits, the programming idiosyncrasies are markedly different for the general circulation model and the near field jet-like thermal discharge.

The problem has therefore been divided into more tractable parts, whose results are to be synthesized for the overall model. Fig. 2.2 shows the various parts and their interrelationships.

- a) A one-dimensional study of the energy equation with no horizontal transport or convective terms is being made. The results will be compared with field data. Conclusions regarding the magnitude and variation of the vertical eddy diffusivity can be made from this study.

The solar radiation boundary condition and the form of the source term in the energy equation should also be available from this study.

- b) A rigid-lid model for the Bay with no tidal effects will be used to give a reasonably clear picture of the wind-driven circulation in the Bay.
- c) A free surface model including tidal boundary conditions will be the final general circulation model. The velocity and temperature fields obtained from this will be used as the far-field solution for the thermal discharge model.
- d) The jet-discharge will be modeled with a horizontal stretching as well as a vertical one to transform the basin to a constant depth - one with the horizontal domain extending from + 1 to - 1 and 0 to + 1, in the transverse and longitudinal directions, respectively.

The combined results of 3 and 4 will constitute the predictions regarding thermal pollution in Biscayne Bay. The programs will be of sufficient generality to be applied to other basins with thermal discharges.

B. THE FAR FIELD

The general circulation for Biscayne Bay has been modeled using both the rigid-lid approximation and free-surface representation. The two parts will be discussed separately.

The system of equations which describe the circulation in a variable density basin are the three Navier-Stokes equations, the energy equation, the conservation of mass equation, and the equation of state. The driving mechanisms are the surface wind stress and the surface heat transfer. The wind stress directly inputs energy into the system by momentum transfer from the wind to the fluid in the basin. The surface heat transfer may cause motions by change of density and consequent buoyancy forces.

1. The Rigid-Lid Model

Fig. 2.3 shows the general coordinate system for which the equations are derived. A left handed cartesian coordinate system has been used, with x, y the horizontal axes and z, the vertical coordinate. z increases downwards with the air-water interface as the origin.

1.1. Assumptions and Approximations

- a) In order to avoid gravity waves, and thereby small time scales and consequent large computation times, the rigid-lid approximation is made. This forces the vertical velocities at the surface to be zero, but allows horizontal velocities. Hag and Lick [19] have developed a criterion for the validity of the rigid-lid approximation. They define a parameter

$$\delta = \frac{4\pi^2 gH}{L^2 f^2} \quad (2-1)$$

and state that for $\beta \rightarrow \infty$ the rigid-lid solution is approximated. Here g is the acceleration due to gravity, f the Coriolis parameter and L and H the horizontal and vertical length scales. They found that the rigid-lid approximation gave almost the same solutions as free-surface models if $\beta > 10$.

- b) The vertical momentum is approximated to the hydrostatic equation. This is quite accurate since the vertical velocities are normally very small. The horizontal length scale is very large compared to the vertical length scale.
- c) The effects of turbulence are modeled by using eddy transport coefficients.
- d) The Boussinesq approximation is made implying that the density variations are small except in the vertical momentum equation in the form of a buoyancy term.

1.2. Basic Equations

The conservative form of the convective terms are presented here. The conservative form results in conservation of mass, momentum and energy and avoids computational instabilities in long term integrations of the time dependent equations. The equations have been stretched in the vertical coordinate using the stretching

$$\eta = z/h(x, y); \quad \begin{matrix} x \rightarrow \alpha \\ y \rightarrow \beta \end{matrix}$$

where h is the depth at any x, y location. This converts the basin to a constant depth one. Now the same number of grid points in the vertical direction may be used at shallow or deep parts of the Bay without using variable grid sizes in the program. The details of the derivations are presented in a report by Sengupta and Lick [19].

The non-dimensional equations are:

Continuity

$$\frac{\partial(hu)}{\partial \alpha} + \frac{\partial(hv)}{\partial \beta} + h \frac{\partial \eta}{\partial \gamma} = 0 \quad (2-2)$$

Momentum

$$\begin{aligned} \frac{\partial(hu)}{\partial t} + \frac{\partial(huu)}{\partial \alpha} + \frac{\partial(huv)}{\partial \beta} + h \frac{\partial(\Omega u)}{\partial \gamma} - \frac{h}{R_B} v^2 \\ = -h \frac{\partial P_s}{\partial \alpha} - h B_x + \frac{1}{Re} \frac{\partial}{\partial \alpha} \left(h \frac{\partial u}{\partial \alpha} \right) + \frac{1}{Re} \frac{\partial}{\partial \beta} \left(h \frac{\partial u}{\partial \beta} \right) \\ + \frac{1}{\epsilon^2 Re} \frac{1}{h} \frac{\partial}{\partial \gamma} \left(A_V^* \frac{\partial u}{\partial \gamma} \right) \end{aligned} \quad (2-3)$$

$$\begin{aligned} \frac{\partial(hv)}{\partial t} + \frac{\partial(huv)}{\partial \alpha} + \frac{\partial(hvv)}{\partial \beta} + h \frac{\partial(\Omega v)}{\partial \gamma} + \frac{h}{R_B} u \\ = -h \frac{\partial P_s}{\partial \beta} - h B_y + \frac{1}{Re} \frac{\partial}{\partial \beta} \left(-h \frac{\partial v}{\partial \beta} \right) \\ + \frac{1}{Re} \frac{\partial}{\partial \alpha} \left(h \frac{\partial v}{\partial \alpha} \right) + \frac{1}{\epsilon^2 Re} \frac{1}{h} \frac{\partial}{\partial \gamma} \left(A_V^* \frac{\partial v}{\partial \gamma} \right) \end{aligned} \quad (2-4)$$

Hydrostatic Equation

$$\frac{\partial p}{\partial \gamma} = Eu (1+f) h \quad (2-5)$$

Energy

$$\begin{aligned} \frac{\partial(hT)}{\partial t} + \frac{\partial(huT)}{\partial \alpha} + \frac{\partial(hvT)}{\partial \beta} + h \frac{\partial(\Omega T)}{\partial \gamma} \\ = \frac{1}{Pe} \frac{\partial}{\partial \alpha} \left(h \frac{\partial T}{\partial \alpha} \right) + \frac{1}{Pe} \frac{\partial}{\partial \beta} \left(h \frac{\partial T}{\partial \beta} \right) + \frac{1}{Pe \epsilon^2} \frac{1}{h} \left(\beta_V^* \frac{\partial T}{\partial \gamma} \right) \end{aligned} \quad (2-6)$$

Equation of State

$$f = f'(T) \quad (2-7)$$

where P_s is the pressure on the rigid-lid

$$\begin{aligned} u &= \tilde{u}/U_{ref}; \quad v = \tilde{v}/U_{ref}; \quad w = \tilde{w}/U_{ref}; \quad t = \tilde{t}/t_{ref}, \\ x &= \tilde{x}/L; \quad y = \tilde{y}/L; \quad z = \tilde{z}/H; \quad \epsilon = H/L; \quad P = \tilde{P}/\rho_{ref} U_{ref}^2; \\ T &= (\tilde{T} - T_{ref})/T_{ref}; \quad \theta = (\tilde{\theta} - \theta_{ref})/\theta_{ref}; \quad A_H^* = A_H/A_{ref}, \\ A_V^* &= A_V/A_{ref}; \quad B_H^* = \rho_H/\rho_{ref}; \quad B_V^* = B_V/\rho_{ref}; \quad t_{ref} = L/U_{ref} \end{aligned}$$

where quantities with subscript 'ref' are reference quantities, H and L are vertical and horizontal length scales. The variables with tilda are dimensional quantities. Also,

$$R_e = \frac{U_{ref} L}{A_{ref}} \sim \text{Reynolds \#}$$

$$\frac{\text{Inertia Force}}{\text{Viscous Force}}$$

$$R_B = \frac{U_{ref}}{fL} \sim \text{Rossby \#} \sim \frac{\text{Inertia}}{\text{Coriolis Force}}$$

$$f = 2 \Omega \sin \phi$$

$$\phi \sim \text{latitude}$$

$$\Omega \sim \text{angular velocity of earth}$$

$$Pr = \frac{A_{ref}}{B_{ref}} \sim \text{Prandtl \#} \sim \frac{\text{Viscous Diffusion}}{\text{Thermal Diffusion}}$$

$$P_e = RePr \sim \frac{U_{ref} L}{B_{ref}} \sim \text{Peclet \#}$$

$$Eu = \frac{gH}{2 U_{ref}^2} \sim \text{Euler \#} \sim \frac{\text{Hydrostatic Pressure}}{\text{Dynamic Pressure}}$$

The conventional vertical velocity is given by

$$W = \gamma \left(u \frac{\partial h}{\partial x} + v \frac{\partial h}{\partial y} \right) + h - 2$$

and

$$B_x = Eu \frac{\partial h}{\partial x} \int_0^y f dy + Eu h \frac{\partial}{\partial x} \int_0^y f dy - Eu \gamma \frac{\partial h}{\partial x} f,$$

$$B_y = Eu \frac{\partial h}{\partial y} \int_0^y f dy + Eu h \frac{\partial}{\partial y} \int_0^y f dy - Eu \gamma \frac{\partial h}{\partial y} f;$$

Equation (2-7) is integrated and substituted in the horizontal momentum equations which are then integrated from $\gamma = 0$ to $\gamma = 1$. The integrated forms of these equations are that cross-differentiated with respect to x , and y and summed. The resulting equation for pressure is

$$\begin{aligned} \frac{\partial^2 P_s}{\partial \alpha^2} + \frac{\partial^2 P_s}{\partial \beta^2} = & \frac{1}{h} \frac{\partial}{\partial \alpha} (-A_{x_1} + A_{x_2} + C_x - X_p) \\ & + \frac{1}{h} \frac{\partial}{\partial \beta} (-A_{y_1} - A_{y_2} + C_y - Y_p) \\ & - h \left\{ \frac{\partial h}{\partial \alpha} \cdot \frac{\partial P_s}{\partial \alpha} + \frac{\partial h}{\partial \beta} \cdot \frac{\partial P_s}{\partial \beta} \right\} - \frac{\partial (2)}{\partial t} \quad (2-8) \end{aligned}$$

REPRODUCIBILITY OF THE
ORIGINAL PAGE IS POOR

where

$$A_{x_1} = \int_0^1 \left\{ \frac{\partial}{\partial \alpha} (h u u) + \frac{\partial}{\partial \beta} (h u v) + h \frac{\partial}{\partial r} (2u) \right\} dr$$

$$A_{x_2} = \frac{h}{R_B} \int_0^1 v dr$$

$$C_x = \frac{1}{Re} \int_0^1 \left\{ \frac{\partial}{\partial \alpha} \left(h \frac{\partial u}{\partial \alpha} \right) + \frac{\partial}{\partial \beta} \left(h \frac{\partial u}{\partial \beta} \right) + \frac{1}{\epsilon^2} \frac{1}{h} \frac{\partial}{\partial r} \left(A_v^* \frac{\partial u}{\partial r} \right) \right\} dr$$

$$X_p = Eu \int_0^1 h \left\{ \frac{\partial h}{\partial \alpha} \int_0^r f dr + h \frac{\partial}{\partial \alpha} \int_0^r f dr - r \frac{\partial h}{\partial \alpha} f \right\} dr$$

and

$$A_{y_1} = \int_0^1 \left\{ \frac{\partial}{\partial \alpha} (h u v) + \frac{\partial}{\partial \beta} (h v v) + h \frac{\partial}{\partial r} (2v) \right\} dr$$

$$A_{y_2} = \frac{h}{R_B} \int_0^1 u dr$$

$$C_y = \frac{1}{Re} \int_0^1 \left\{ \frac{\partial}{\partial \alpha} \left(h \frac{\partial v}{\partial \alpha} \right) + \frac{\partial}{\partial \beta} \left(h \frac{\partial v}{\partial \beta} \right) + \frac{1}{\epsilon^2} \frac{1}{h} \frac{\partial}{\partial r} \left(A_v^* \frac{\partial v}{\partial r} \right) \right\} dr$$

$$Y_p = Eu \int_0^1 h \left\{ \frac{\partial h}{\partial \beta} \int_0^r f dr + h \frac{\partial}{\partial \beta} \int_0^r f dr - r \frac{\partial h}{\partial \beta} f \right\} dr$$

The last term in equation (2-8) is the Hirt and Harlow [20] correction term. This is evaluated by a backward difference scheme in time with the present time set equal to zero. This is necessary because the Poisson equation is solved by iterative technique leading to errors. If they are not corrected, the continuity equation is not satisfied leading to accumulation or loss of fluid from the system.

Equations (2-2) to (2-8) form the system of equations which together with the appropriate boundary conditions constitute the mathematical model.

1.3. Boundary Conditions

The boundary conditions may be written separately for the air-water interface, the sidewalls and the bottom of the basin. At the air-water interface the boundary condition on the momentum equations are obtained in the form of wind stress. This may be determined from experimental correlations. Edinger and Geyer [21] have determined the heat flux relations at the air-water interface. They define an equilibrium temperature as that at which no heat flux takes place at the surface and relate heat flux directly to the difference between the surface temperature and the equilibrium temperature.

$$\text{Heat flux} = \Delta Q = K_s (\bar{T}_E - \bar{T}_S)$$

in dimensional form, where K_s is the surface heat transfer coefficient and \bar{T}_S the dimensional surface temperature.

$$\text{Now} \quad \Delta Q = B_g \frac{\partial \tilde{T}}{\partial \tilde{z}} \Big|_{\text{at surface}}$$

$$\text{or} \quad \frac{\partial \tilde{T}}{\partial \tilde{z}} = \frac{K_s}{B_g} (\bar{T}_E - \bar{T}_S)$$

The conditions on the sidewalls are no-slip, and no normal velocity, for the momentum equations except $w \neq 0$, due to the hydrostatic equation. The heat flux is approximated to be zero.

However, the heat flux may be also specified as a function of the wall temperature and some heat transfer coefficients.

At the bottom, the conditions of no-slip and no normal velocity are applicable. The energy equation has a boundary condition of zero heat flux. As discussed for the side walls it may be equated to non-zero values also.

Therefore, the boundary conditions are in summary:

Normal derivatives

$$\frac{\partial T}{\partial \alpha} = \frac{\partial T}{\partial \alpha} - \frac{\gamma}{h} \frac{\partial h}{\partial \alpha} \cdot \frac{\partial T}{\partial \gamma} = 0$$

or

$$\frac{\partial T}{\partial \beta} = \frac{\partial T}{\partial \beta} - \frac{\gamma}{h} \cdot \frac{\partial h}{\partial \beta} \cdot \frac{\partial T}{\partial \gamma} = 0$$

The boundary conditions on the pressure equation are obtained by evaluating the values of $\frac{\partial P_s}{\partial \alpha}$ and $\frac{\partial P_s}{\partial \beta}$ from the momentum equations. Therefore, the pressure solution requires a solution to the Neumann problem. The solution is unique to within a constant. However, since only the derivatives of pressure enter the momentum equations, the actual values of the pressure solution surface are unimportant as long as the shape is correct. At the surface

at $\gamma = 0$

$\Omega = 0$ Rigid-Lid

$$\frac{\partial u}{\partial \gamma} = \left(\frac{h H}{U_{ref} A_V} \right) \tau_{zx} ; \quad \frac{\partial T}{\partial \beta} = \left(\frac{h H k_s}{B_z} \right) (T_E - T_S) ;$$

$$\frac{\partial v}{\partial \gamma} = \left(\frac{h H}{U_{ref} A_V} \right) \tau_{zy} ;$$

where τ_{zx} and τ_{zy} are wind stresses in the x and y - directions respectively.

At the bottom of the basin:

at $\gamma = 1$

$$\begin{aligned}\Omega &= 0 \\ u &= 0 \\ v &= 0 \\ \frac{\partial T}{\partial y} &= 0\end{aligned}$$

On lateral walls:

$$\begin{aligned}u &= 0 \\ v &= 0 \\ \Omega &\neq 0\end{aligned}$$

1.4. Method of Solution

Fig. 2.4 shows the grid system and the arrangement of variables. u and v are located on integral nodes (i, j, k) on the horizontal or x, y plane. P , w , and T are located at half grid points $(i + 1/2, j + 1/2, k)$. The arrangement is repeated in the z or y direction, represented by K .

The finite difference equation for the momentum and energy equation may be represented in the general form.

$$\frac{u^n + 1 - u^n}{\Delta t} = (\text{convection})^n + (\text{pressure})^n + (\text{viscous})^n$$

Where u may be replaced by v or T (for the T equation the pressure term is not there). The spatial derivatives are central differenced.

The pressure equation is approximated by a five-point scheme and solved by Liebmann relaxation procedure.

The relevant stability criterion are:

Convection

$$C_x \left(\frac{\Delta \bar{t}}{\Delta \bar{x}} \right) + C_y \left(\frac{\Delta \bar{t}}{\Delta \bar{y}} \right) + C_z \left(\frac{\Delta \bar{t}}{\Delta \bar{z}} \right) < 1$$

Diffusion

$$D_x \frac{\Delta \bar{t}}{(\Delta \bar{x})^2} + D_y \frac{\Delta \bar{t}}{(\Delta \bar{y})^2} + D_z \frac{\Delta \bar{t}}{(\Delta \bar{z})^2} < 1/2$$

l_x , l_y , and l_z may be interpreted as the maximum values of u , v and w in the domain and D_x , D_y , D_z as the kinematic eddy transport coefficients in x , y and z directions.

Fig. 2-5 shows the flow chart for the steps in the solution algorithm summarized below:

1. Using values at time step n , calculate the forcing term for the pressure equation.
2. Solve the pressure equation iteratively.
3. Calculate u , v from the momentum equations.
4. Calculate Ω from the continuity equation using u , v at $n + 1$.
5. Calculate T from the energy equation.
6. Calculate ρ from the empirical equation of state.

The values at $(n + 1)$ have now been obtained. Repeat the procedure for $(n + 2)$ using value at $(n + 1)$.

2. The Free - Surface Model

The mean ocean tide for Biscayne Bay is about 2.44 ft. Since, the maximum depth of the Bay is around 12 ft, the tidal effects are significant. To model the effects of tides a free-surface model is imperative.

Fig. 2-6 shows the general coordinate system for which the equations are derived. Freeman et al [11] have derived the governing equations for a free-surface model. Their procedure is followed here.

All the assumptions of the rigid-lid model apply for the free-surface model except for the zero vertical velocity condition at the surface.

2.1. Basic Equations

A vertical stretching of the form

$\gamma = Z/H$ is used

where $Z = Z(x, y, z, t)$ is the position relative to the free surface.

$H = H(x, y, t)$ is the depth relative to the free surface.

$Z = z + \eta(x, y, t)$ where z is the position relative to the mean water level and η the free-surface elevation measured positively upwards also

$H = h(x, y) + \eta(x, y, t)$ where h is the depth of the basin with respect to the mean water level. γ is 0 at the free-surface and 1 at the bottom.

As a result of the above transformations we can define pressure gradients as follows: (in dimensional form for easier understanding)

$$\left(\frac{\partial p}{\partial x}\right)_{z, y, t} = \left(\frac{\partial p}{\partial x}\right)_{r, y, t} - \rho g \left(\gamma \frac{\partial H}{\partial x} - \frac{\partial \eta}{\partial x}\right)_{r, y, t} \quad (2-10)$$

$$\left(\frac{\partial p}{\partial y}\right)_{z, x, t} = \left(\frac{\partial p}{\partial y}\right)_{r, x, t} - \rho g \left(\gamma \frac{\partial H}{\partial y} - \frac{\partial \eta}{\partial y}\right)_{r, x, t} \quad (2-11)$$

an appropriate form of the continuity equation is

$$\begin{aligned} \left(\frac{\partial H}{\partial t}\right)_{x, y, r} + \left(\frac{\partial(Hu)}{\partial x}\right)_{y, r, t} \\ + \left(\frac{\partial(Hu)}{\partial y}\right)_{x, r, t} + H \left(\frac{\partial \Omega}{\partial \gamma}\right)_{x, y, t} = 0 \end{aligned} \quad (2-12)$$

The horizontal momentum equations may be written as

$$\begin{aligned} \left(\frac{\partial(Hu)}{\partial t}\right)_{x, y, r} + \left(\frac{\partial(Huu)}{\partial x}\right)_{y, r, t} + \left(\frac{\partial(Huv)}{\partial y}\right)_{x, r, t} \\ + H \left(\frac{\partial(Hu)}{\partial \gamma}\right)_{x, y, t} = H \left[-\frac{1}{\rho} \left(\frac{\partial p}{\partial x}\right)_{y, r, t} \right. \\ \left. + g \left(\gamma \frac{\partial H}{\partial x} - \frac{\partial \eta}{\partial x}\right)_{y, r, t} - f v \right] \\ + A_H \left(\frac{\partial}{\partial x} \left(H \frac{\partial u}{\partial x}\right)\right)_{y, r, t} + A_H \left(\frac{\partial}{\partial y} \left(H \frac{\partial u}{\partial y}\right)\right)_{x, r, t} \\ + \frac{1}{\rho} \left(\frac{\partial}{\partial \gamma} \left(\rho A_H \frac{\partial u}{\partial \gamma}\right)\right)_{x, y, t} \end{aligned} \quad (2-13)$$

$$\begin{aligned} & \left(\frac{\partial(Hu)}{\partial t} \right)_{x,y,r} + \left(\frac{\partial(Hu)}{\partial x} \right)_{y,r,t} + \left(\frac{\partial(Hu)}{\partial y} \right)_{x,r,t} \\ & + H \left(\frac{\partial(\Omega u)}{\partial r} \right)_{x,y,t} = H \left[-\frac{1}{f} \left(\frac{\partial P}{\partial y} \right)_{x,r,t} \right. \\ & \left. + g \left(r \frac{\partial H}{\partial y} - \frac{\partial r}{\partial y} \right)_{x,r,t} + f u \right] + A_H \left(\frac{\partial}{\partial x} \left(H \frac{\partial u}{\partial x} \right) \right)_{y,r,t} \\ & + A_H \left(\frac{\partial}{\partial y} \left(H \frac{\partial u}{\partial y} \right) \right)_{x,r,t} + \frac{1}{f} \left(\frac{1}{H} \frac{\partial}{\partial r} \left(f A_V \frac{\partial u}{\partial r} \right) \right)_{x,y,t} \end{aligned}$$

REPRODUCIBILITY OF THE
ORIGINAL PAGE IS POOR

(2-14)

The energy equation may be written as

$$\begin{aligned} & \left(\frac{\partial(HT)}{\partial t} \right)_{x,y,r} + \left(\frac{\partial(HuT)}{\partial x} \right)_{y,r,t} + \left(\frac{\partial(HuT)}{\partial y} \right)_{x,r,t} \\ & + H \left(\frac{\partial(\Omega T)}{\partial r} \right)_{x,y,t} = B_H \left(\frac{\partial}{\partial x} \left(H \frac{\partial T}{\partial x} \right) \right)_{y,r,t} + B_H \left(\frac{\partial}{\partial y} \left(H \frac{\partial T}{\partial y} \right) \right)_{x,r,t} \\ & + \frac{1}{f} \left(\frac{1}{H} \frac{\partial}{\partial r} \left(f B_V \frac{\partial T}{\partial r} \right) \right)_{x,y,t} \end{aligned}$$

(2-15)

By integrating (2-12) over the height, we get

$$\frac{\partial H}{\partial t} = - \int_0^1 \left(\frac{\partial(Hu)}{\partial x} + \frac{\partial(Hu)}{\partial y} \right) r dr \quad (2-16)$$

if we integrate (2-12) from 0 to r , we get

$$\Omega = \frac{1}{H} \int_0^r \left(\frac{\partial(Hu)}{\partial x} + \frac{\partial(Hu)}{\partial y} \right) r dr + \frac{r}{H} \int_0^1 \left(\frac{\partial(Hu)}{\partial x} + \frac{\partial(Hu)}{\partial y} \right) r dr \quad (2-17)$$

The hydrostatic relation can be integrated from $r = 0$ to $r = r$ to obtain

$$P(r) = P(0) + gH \int_0^r \rho(r) dr \quad (2-18)$$

also

$$w = \frac{dz}{dt} = H \frac{dr}{dt} + (r-1) \frac{d\eta}{dt} + \frac{dh}{dt} \quad (2-19)$$

The above set of equations is sufficient to model the free-surface general circulation in Biscayne Bay.

2.2. Boundary Conditions

The boundary conditions are the same as that for the rigid-lid model except that now vertical velocities can be non-zero at the surface. Also we have to specify the wave height at tidal inlets.

The new variable η introduces a boundary condition from continuity;

$$\frac{\partial \eta}{\partial t}(x_B, y, t) = - \left(\frac{\partial(Hu)}{\partial y}(x_B, y, 0, t) \right)_{x, y, t} \quad (2-20)$$

$$\frac{\partial \eta}{\partial t}(x, y_B, t) = - \left(\frac{\partial(Hu)}{\partial x}(x, y_B, 0, t) \right)_{x, y, t} \quad (2-21)$$

x_B , and y_B signify lateral walls.

At tidal inlets $\frac{\partial \eta}{\partial t}$ is known. Therefore the relation between velocities at boundary and the next adjacent interior point is specified. At solid walls u, v are zero. Therefore since interior values can be calculated, $\frac{\partial \eta}{\partial t}$ is automatically specified by equations (2-20) and (2-21).

2.3. Method of Solution

A staggered grid of the kind used for the rigid-lid model is used here. There is one extra variable H or η , defined at half-grid points.

The equations are forward differenced in time and central differenced in space. The integration procedure is as follows:

- a) Calculate H and η at $n + 1$ using values at n
- b) Calculate P at $n + 1$
- c) Calculate T at $n + 1$ using values at n
- d) Calculate u, v at $n + 1$ using values at n
- e) Calculate ρ at $n + 1$ using values at $n + 1$ of other variables
- f) Calculate w using ρ .
- g) Calculate ρ at $n + 1$ using T at $n + 1$

Repeat the procedure for next time step. Fig 2.7 shows the flow chart.

3. One-Dimensional Analysis

The vertical eddy transport coefficient is a dominant property of the flow field. The vertical structure is largely influenced by the value and variation of the vertical eddy transport coefficient.

If we neglect the convective and horizontal diffusion terms from the energy equation, we obtain a one-dimensional form of the equation.

$$\frac{\partial \tilde{T}}{\partial z} = B_v \frac{\partial^2 \tilde{T}}{\partial z^2} + Q \text{ - (dimensional). form . (Q ~ Source term) (2-22)}$$

For the constant K_v case an analytical solution can be obtained for the above equation in the domain $0 \leq z \leq H$, $t \geq 0$, given $\tilde{T}(0)$. Where H is the depth of the basin. The boundary conditions being heat transfer coefficient at the surface and bottom.

$$\text{i.e. at } \tilde{z} = 0 \quad \frac{\partial \tilde{T}}{\partial \tilde{t}} = \frac{K_s}{B_z} (\tilde{T}_E - \tilde{T}_S)$$

where $B_z = \rho C B_v$

at $\tilde{z} = H$. $\partial \tilde{T} / \partial \tilde{z} = 0$. -(adiabatic.)

All the other notations are the same as in previous discussion.

However, in most situations B_v varies with depth and density stratification. The non-linear interaction of wind generated turbulence and buoyancy generated turbulence may cause phenomena like the formation of a thermocline.

One much used model for the eddy diffusivity is the Richardson number model. The Richardson number is defined as

$$Ri = \frac{g \frac{\partial \bar{\rho}}{\partial \bar{z}}}{\bar{\rho} \left(\frac{\partial \bar{u}}{\partial \bar{z}} \right)^2} ;$$

g is the acceleration due to gravity, $\partial \bar{\rho} / \partial \bar{z}$ the local density gradient, and $\partial \bar{u} / \partial \bar{z}$ the vertical gradient of velocity. The coordinate \bar{z} is positive downwards.

There are many empirical formula relating the eddy transport coefficients with the Richardson number. Munk and Anderson [22] and Sunderam and Rehm [23] have discussed some of these relations. One suitable form is

$$B_V = B_{V_0} (1 + m Ri)^{-n}$$

B_{V_0} is the value with no density stratification.
 m and n are empirical constants.

The source term is largely determined by the solar absorption characteristics and thereby by the turbidity of the basin. Harleman and Dake [24] have determined some exponential forms for Q variation with z . They show that the form of Q variation with depth can greatly enhance the formation of the thermocline.

The purpose of the one-dimensional investigation is to find the value of B_{V_0} and some simple law that gives the variation of B_V with z . Also, some idea of the form of Q can be obtained.

Equation (2-22) can be very simply solved by finite-difference methods. The results can then be compared with field data collected in Biscayne Bay. By an empirical process of matching numerical results with field data the values of B_{V_0} and the forms of B_V and Q can be determined.

Some preliminary results for the one-dimensional case are shown in Fig. 2.8. The results for a variable K_V are shown for heating to 30 days. The initial temperature difference between the ambient and the fluid media is 20°C . It can be seen that after 30 days the beginnings of a thermocline can be seen at about mid-depth. The profiles for constant K_V however show the regular conduction type profile with no thermocline behavior.

C. THE NEAR FIELD

A thermal plume issuing into a basin has regimes of different fluid mechanic characteristics. Right at the mouth of the discharge the flow is totally dominated by a jet like behavior. The jet then spreads with turbulent mixing at the edges. The convective transport is quite dominant. The bouyancy of the jet causes it to move upwards. Still further downstream the general circulation becomes the dominant force. The hot water from the jet forms a thin layer at the surface and spreads under the action of diffusion and general circulation.

For our present study we have defined two regions namely the "near field" and the "far field". The far field is that region where the temperature and velocity anomaly is caused by the discharge. The "near field" is the region influenced by the thermal discharge. The "far field" solution, however, affects the "near field" although not vice versa.

The governing equations are the same as derived for the "far field". The boundary conditions are different. A typical domain is shown in Figure [2.9]. One side of the domain consists of a solid boundary at which no-slip conditions are satisfied except at the discharge point where velocity and temperature profiles are specified. The dotted lines indicate the far field boundary. Here the results from the far field solutions are specified. However, this boundary condition has to be constantly updated by extrapolation from the interior so as to satisfy conservation of mass, momentum and heat in the domain.

The method of solution is also as specified in the far field discussions. The flow charts being shown in Figures [2.5] and [2.7]. The two different approaches namely free surface and rigid-lid are applicable for the jet problem also. For the mainland shore of Biscayne Bay near field modeling may be done by rigid-lid approximation owing to the sheltered nature of the bay. However, at places like Hutchinson Island a free surface model is imperative because of direct access to ocean tide.

D. SOME RIGID-LID RESULTS

The rigid-lid model will be used to obtain some preliminary understanding of the general wind driven circulation in Biscayne Bay.

Fig. 2.10 shows the horizontal grid system used to approximate the shore-line of the Bay. No such rectangular fitting is necessary in the vertical direction owing to the mapping of the Bay to a constant depth basin.

1. Constant Depth Rectangular Basin

The Bay was approximated to a rectangular constant depth basin of extent 25 Km x 8 Km x 4M. Two cases were solved, one with a vertical eddy viscosity to $5\text{cm}^2/\text{sec}$ and the other with $1\text{cm}^2/\text{sec}$. The horizontal eddy viscosity and windstress were $10^4\text{cm}^2/\text{sec}$ and 1 dynes/cm^2 respectively.

The time to reach steady state was about 5 hours for the higher vertical viscosity case and 7 hours for the lower viscosity case. There was very little variation with horizontal location. This is expected for a constant depth basin where Coriolis forces are not too dominant.

Fig. 2.11 shows the Ekman spiral for the cases solved. It is seen that for the higher viscosity case the Coriolis effect is almost negligible with velocities lying in the plane of the wind stress. For the lower viscosity case the transverse velocities owing to Coriolis effect are somewhat more pronounced. The top third of the basin has velocities in the general direction of the wind stress with back-flow in the lower region.

2 Variable Depth Closed Basin - No Tidal Influence

The solutions for the variable depth basin were obtained by using the governing equations in the vertically stretched co-ordinate system. Since the governing equations in the stretched system have extra terms, a completely different program had to be developed. A Dufort-Frankel scheme was used on the viscous terms. This was necessary owing to the relatively small vertical grid spacings at the shallow areas of the Bay. This procedure relaxes the diffusive stability criterion.

The basin was assumed closed and tidal effects were ignored. The purpose of the investigation here is to find the wind-driven circulation pattern in the Bay. Later tidal fluxes will be introduced to study the modifications caused by ocean tide.

A vertical eddy viscosity of $5\text{cm}^2/\text{sec}$. was assumed. The wind stress magnitude was taken to be $.1\text{ dynes/cm}^2$. Two cases have been solved. One for wind from the north, the other for wind from the southeast. The average wind during summer and spring in Miami is from the southeast and is at 5 miles per hour. Qualitative assessment of circulation for intermediate wind directions can be made from the results of these two cases.

Fig. 2.12 shows some of the representative non-dimensional numbers for the Bay. The relative importance of various terms in the governing equation is thereby illustrated.

2.1 Wind From North

Fig. 2.13 shows the surface velocities at steady state with wind from the north at about 5 miles per hour. The velocities vary significantly in the domain. The variation of velocity direction and magnitude is as a result of a number of effects. The outline of the Bay guides the current near the shoreline. The bottom slopes tend to influence the velocity, and the local depth of the Bay is significant also. The shallower regions have smaller velocities. This is seen in the shoal areas and near the shore. The reduction of velocity near the shore is caused mainly by the smaller depth rather than by the shore boundary-layers. Estimates by Sengupta and Lick [9] have indicated that the sidewall boundary layers are quite thin for similar situations and do not extend to as far as the nearest interior node (.8 kilometers from the shore). Fig. 2.14 shows the velocities at a depth of 2 meters from the surface. There are no velocity vectors in large parts of the domain since the Bay is less than 2 meters deep in those parts. The return flow can be clearly seen.

A cross-sectional view of the velocity field indicates a cell like structure. Fig. 2.15 shows a section through J=7 (refer to Fig. 2.16). It can be seen that the surface velocities are in the direction of the wind stress. Except for the top third at each location the flow is in the opposite direction indicating a return flow. There is sharp upwelling at the near shore region. Wherever there is sharp change of bottom depth, terms of the form $\partial u/\partial x$ become significant resulting in vertical velocities to satisfy continuity.

It is very important to note that at point A in Fig. 2.15 there is close proximity of upwelling and downwelling. The two cell-like circulation patterns divide the Bay.

This indicates that fluid in the region left of A is not exchanged with fluid to the right of A with any degree of facility.

Fig. 2.16 shows a section through J=9. A similar kind of flow as was discussed above may also be seen here with the basin being divided into two parts at point A.

It is evident that shoals are regions which may divide the bay into separate circulation regions under proper wind conditions.

2.2 Wind from Southeast

The prevailing winds during spring and summer are from the southeast. The surface velocities for this case are shown in Fig. 2.17 . The velocities are approximately in the direction of the wind. The magnitude of the velocities vary with depth and are smaller near-shore and in shoal regions. It is interesting to note the effect of bottom slope. In some parts near the mainland shore the velocities are almost parallel to the shore and not in the direction of the wind. The return flow can be seen in Fig. 2.18 which shows the velocities at a depth of 2 meters.

Fig. 2.19 shows a vertical cross-section of the Bay along J=8. The cell-like circulation pattern is quite clear with a demarcation point between the cells at point A. The effect of shoals is thus quite clear. Fig. 2.20 shows the velocities at section J=9. Here again it is seen that the top quarter of the bay has velocities in the direction of the wind component with the deeper regions being a region of return flow. Vertical velocities are seen in regions of large bottom slopes. Fig. 2.21 shows vertical sections at I=7 and I=11. These east-west sections also show a cell-like circulation pattern. The comments regarding the regions of upwelling and downwelling are the same as before.

The circulation patterns discussed in this chapter are typical and represent the basic nature of the wind driven circulation in Biscayne Bay. It is important to note that the ocean tides will greatly alter the flow patterns computed by the present study. Inclusion of tidal effects and free-surface modeling will result in more realistic flow patterns.

LIST OF SYMBOLS

A_H	horizontal kinematic eddy viscosity
A_V	vertical kinematic eddy viscosity
A_Z	vertical eddy viscosity
A_{ref}	reference kinematic viscosity
A_V^*	A_V / A_{ref}
B_H	horizontal diffusivity
B_V	vertical diffusivity
B_{ref}	reference diffusivity
B_V^*	B_V / B_{ref}
c_p	specific heat at constant pressure
Eu	Euler number
f	coriolis parameter
g	acceleration due to gravity
h	depth at any location in the basin
H	reference depth
k	thermal conductivity
k_s	surface heat transfer coefficient
L	horizontal length scale
P	pressure
P_s	surface pressure
Pr	turbulent Prandtl number
Pe	Peclet number
Q^*	heat source or sinks
Re	Reynolds number
Ri	Richardson number
T	temperature
T_{ref}	reference temperature
T_E	equilibrium temperature

t time
t_{ref} reference time
u velocity in x direction
v velocity in y direction
w velocity in z direction
x horizontal co-ordinate
y horizontal co-ordinate
z vertical co-ordinate

Greek Letters:

α horizontal co-ordinate in stretched co-ordinate system
 β horizontal co-ordinate in stretched system
 γ vertical co-ordinate in stretched system
 μ absolute viscosity
 ρ density
 ϕ dissipation term in energy equation

Superscripts:

($\overline{\quad}$) time averages
(\sim) dimensional mean quantity
($'$) dimensional fluctuating quantity
(\quad)_{ref} reference quantity

LIST OF FIGURES

- 2. 1 Map showing the general area of Biscayne Bay
- 2. 2 Interrelationships of sub-programs
- 2. 3 The co-ordinate system for the rigid-lid model
- 2. 4 Grid-system and arrangement of variables
- 2. 5 Flow chart for rigid-lid computation
- 2. 6 The co-ordinate system for the free-surface model
- 2. 7 Flow chart for free-surface computation
- 2. 8 Vertical temperature profile
- 2. 9 Near field model
- 2.10 Horizontal grid system for Biscayne Bay
- 2.11 Velocity profiles in Biscayne Bay; constant depth approximation
- 2.12 Representative parameters for Biscayne Bay
- 2.13 Surface velocities in Biscayne Bay with wind from the north
- 2.14 Velocities at a depth of 2 meters with wind from the north
- 2.15 Velocities at section J=7 with wind from the north
- 2.16 Velocities at section J=9 with wind from the north
- 2.17 Surface velocities with wind from southeast
- 2.18 Velocities at a depth of 2 meters with wind from the southeast
- 2.19 Velocities at section J=8 with wind from the southeast
- 2.20 Velocities at section J=9 with wind from the southeast
- 2.21 Velocities at section I=7 and I=11 with wind from the southeast

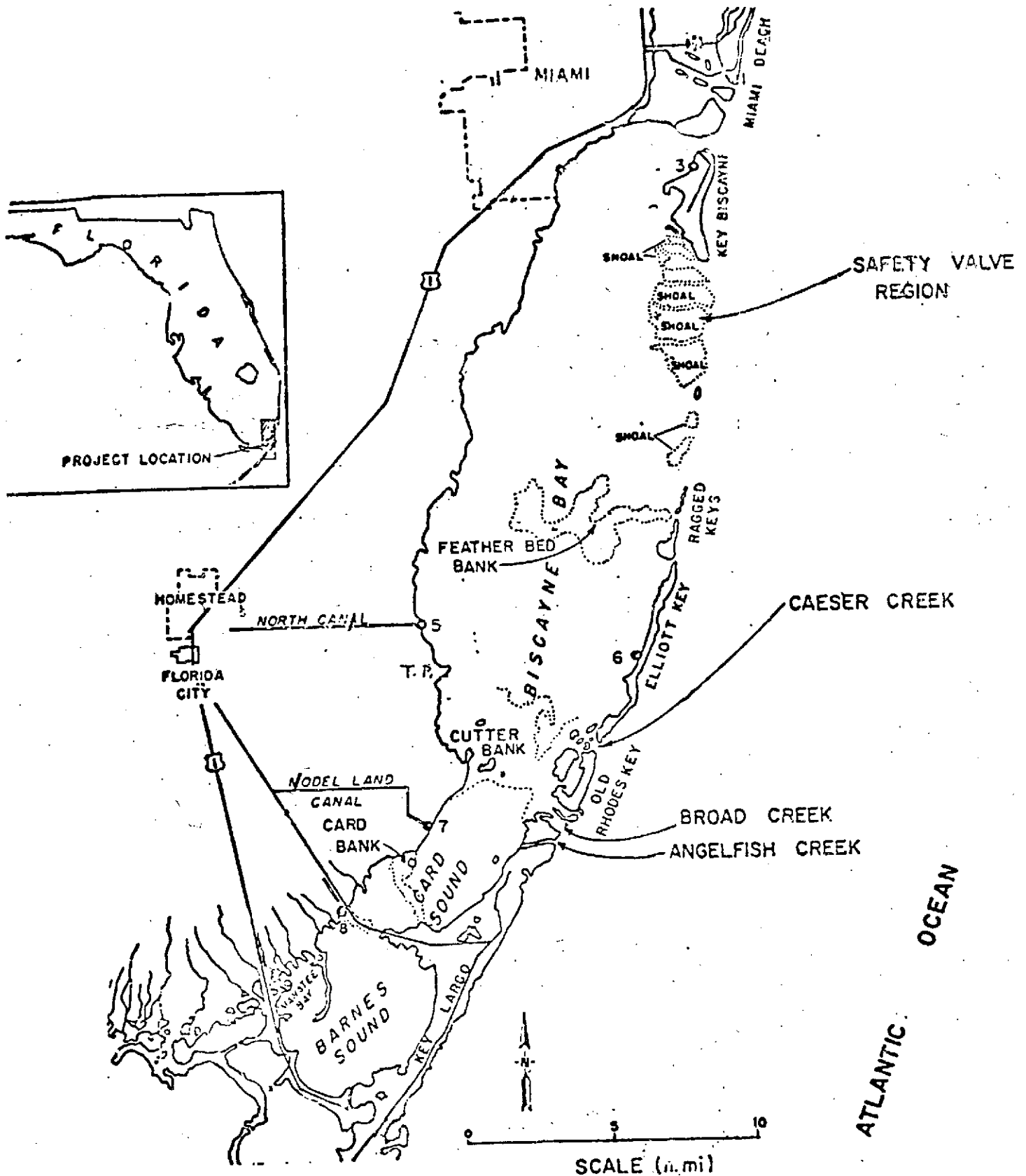


Figure 2-1 Map showing the general area of Biscayne Bay

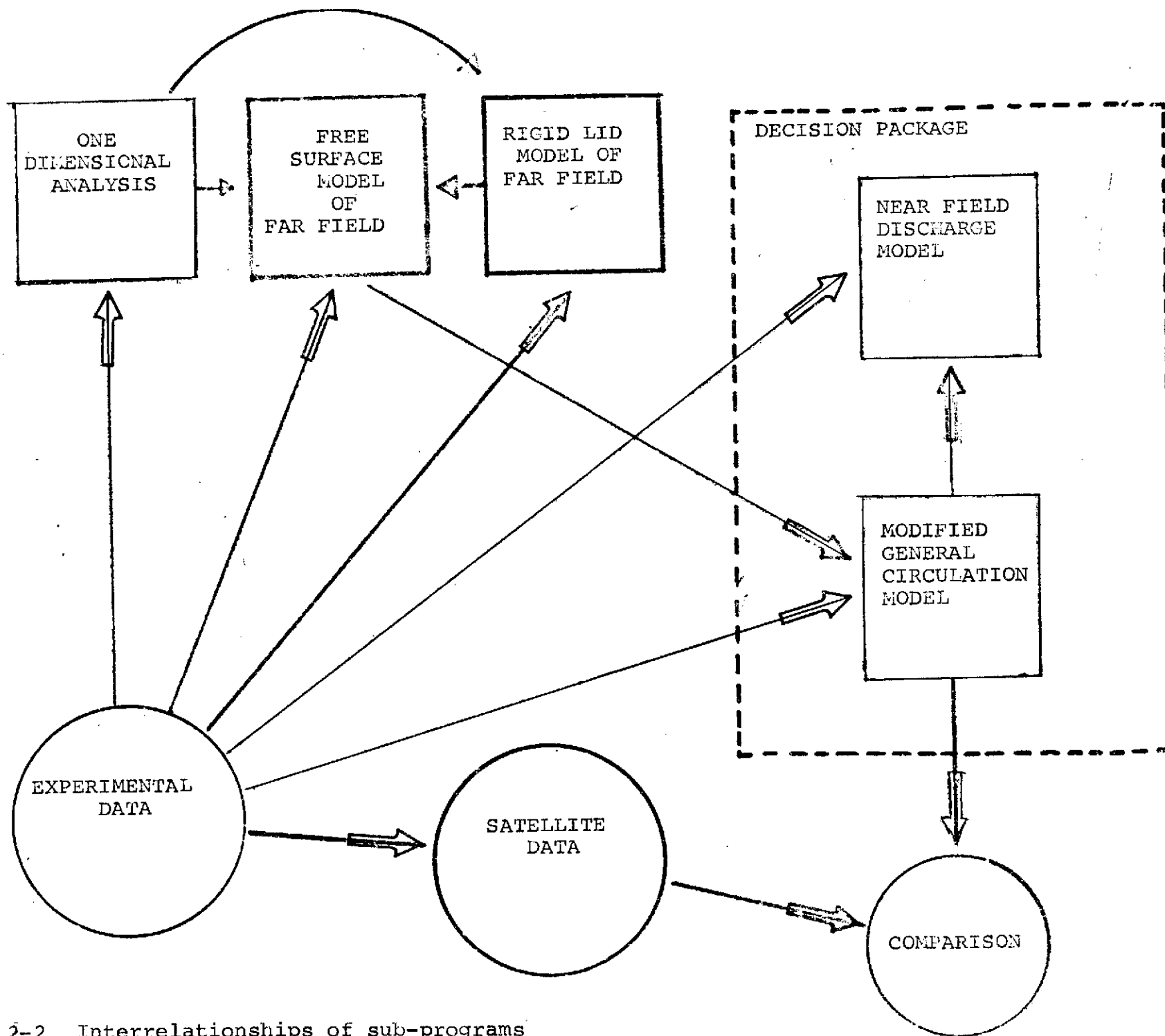


Figure 2-2 Interrelationships of sub-programs

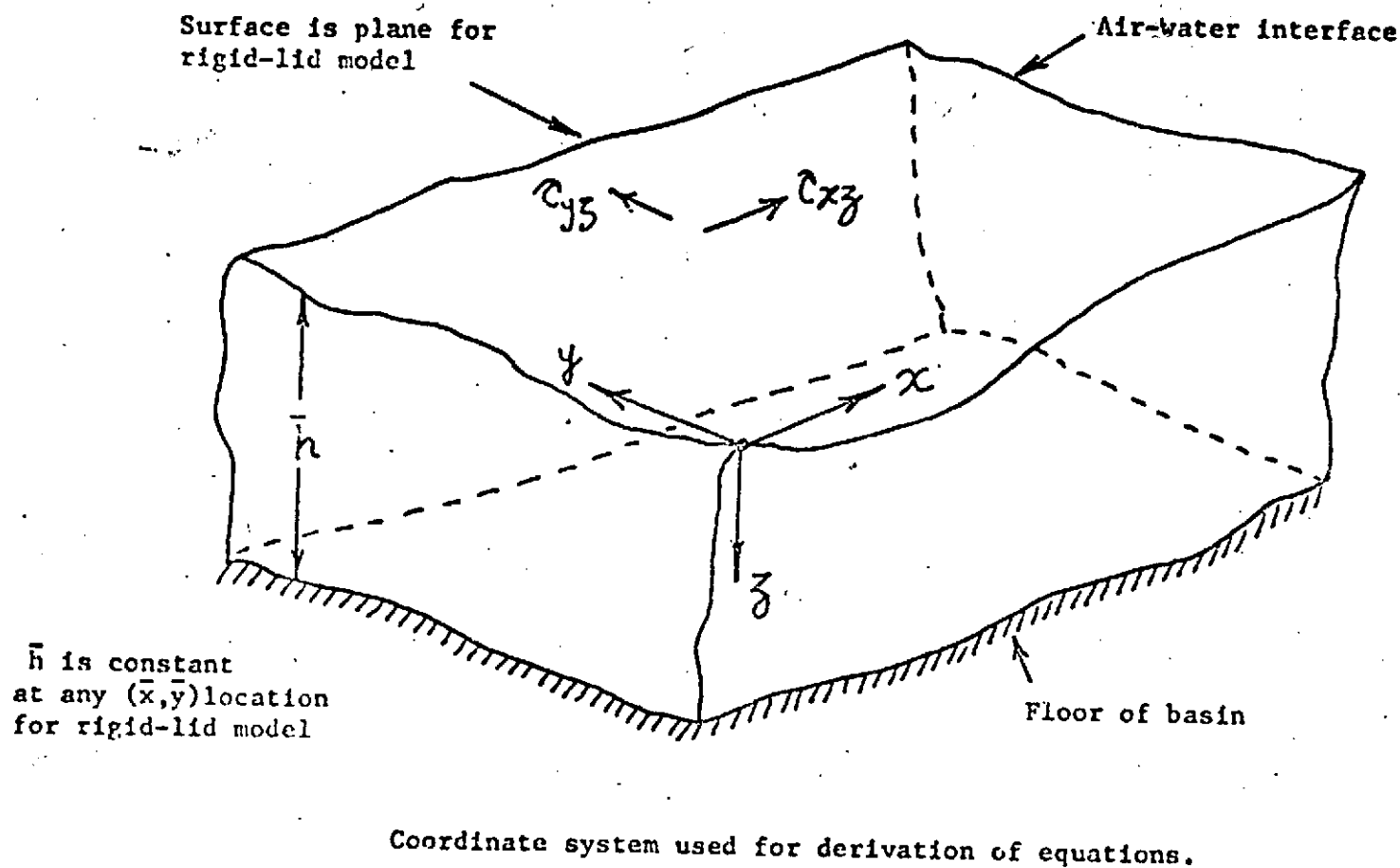
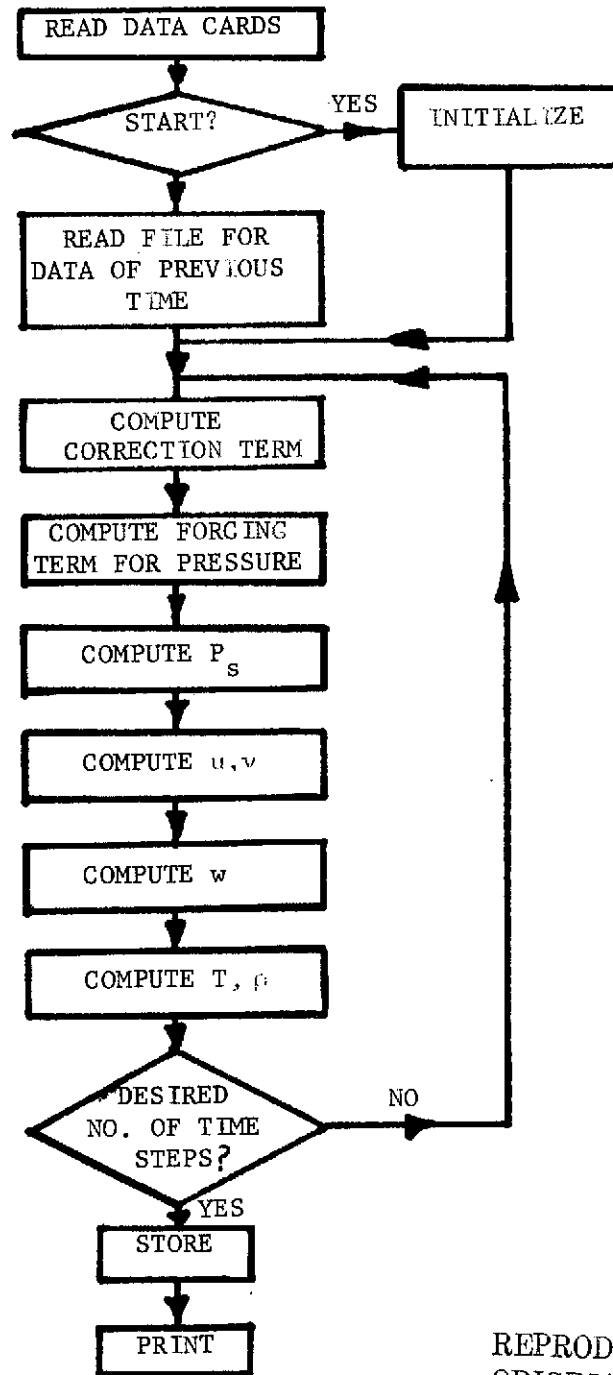


Figure 2.3 The Coordinate system for Rigid-lid model.

REPRODUCIBILITY OF THE
ORIGINAL PAGE IS POOR



REPRODUCIBILITY OF THE
ORIGINAL PAGE IS POOR

Figure 2.5 Flow Chart for Rigid-Lid Computation.

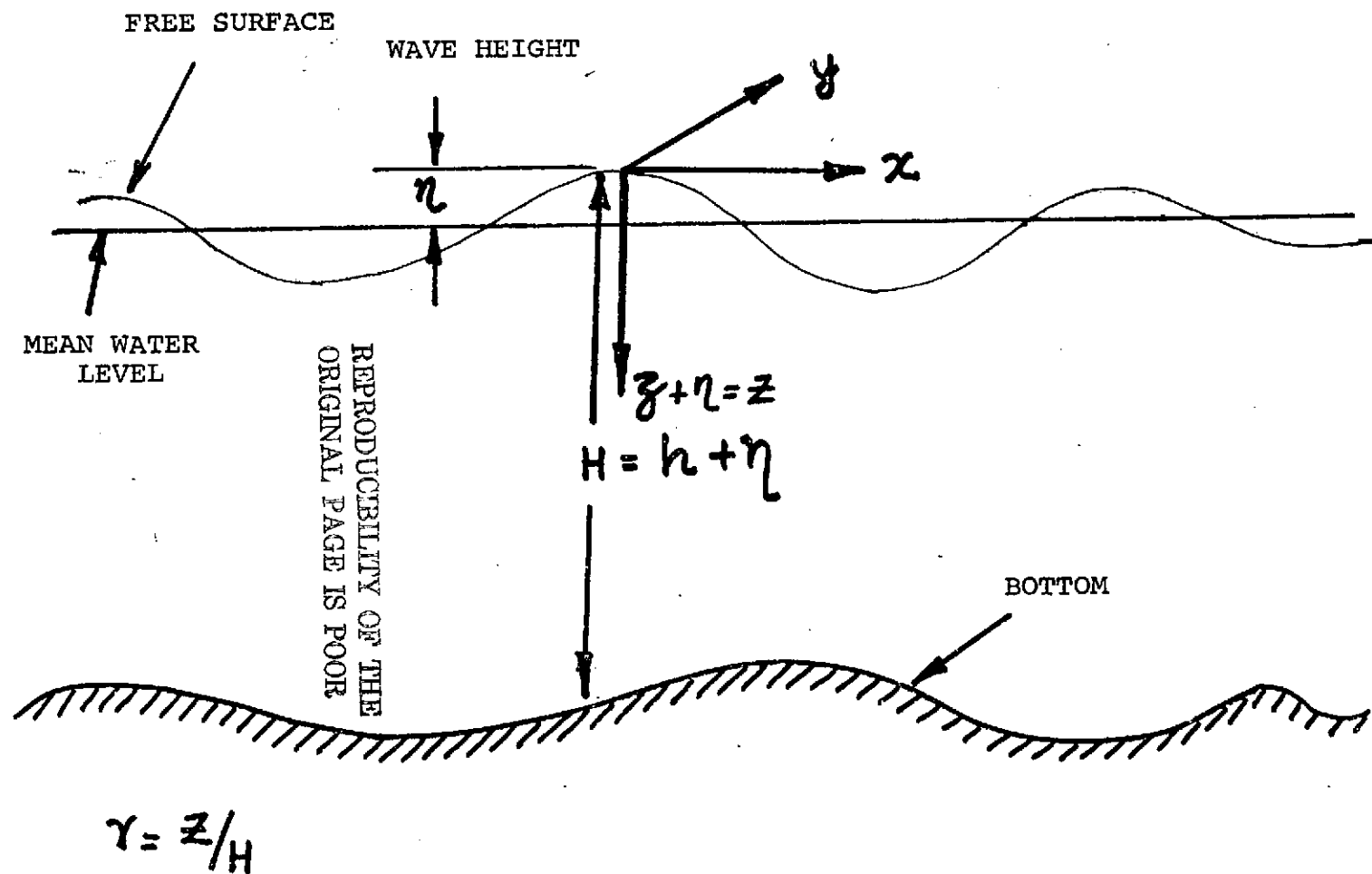


Figure 2-6 The Coordinate System for the Free-Surface Model

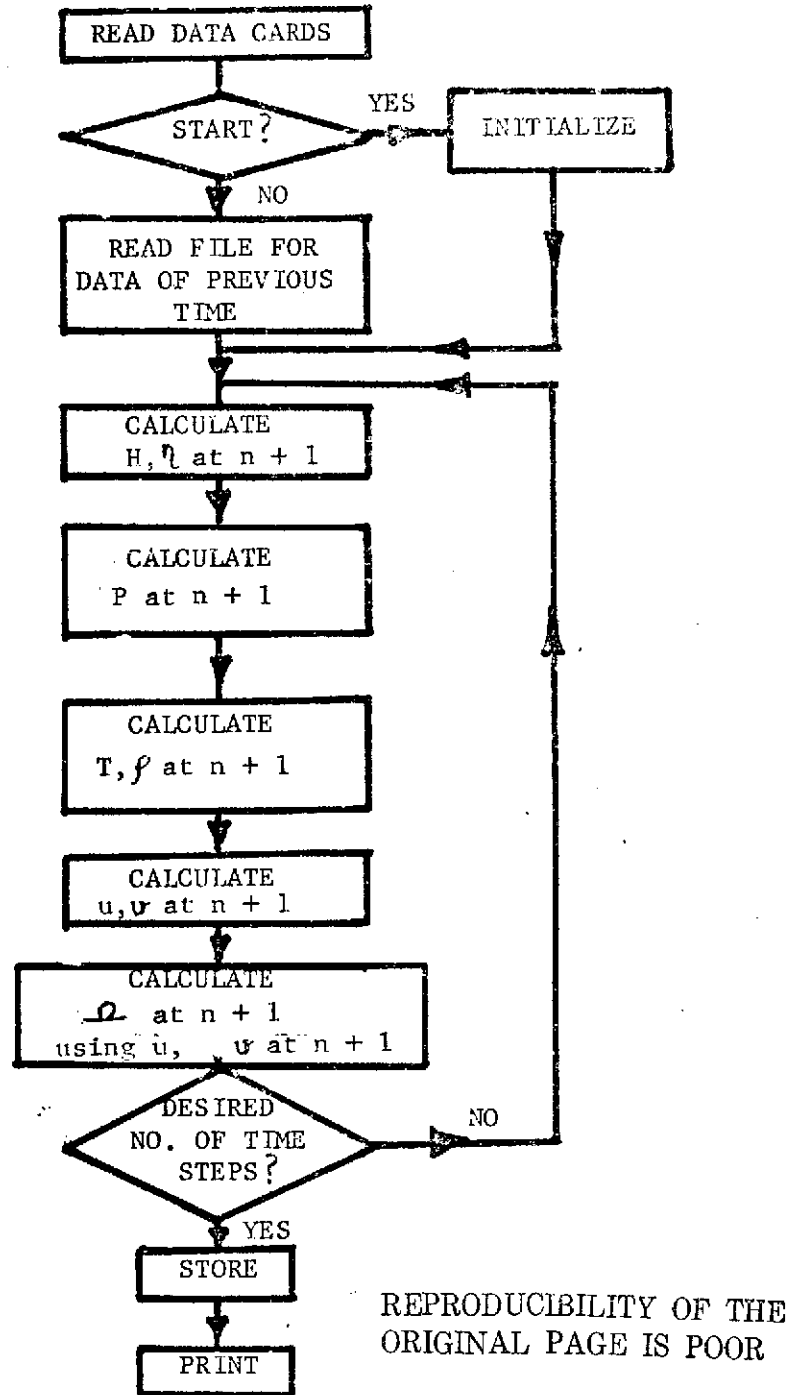
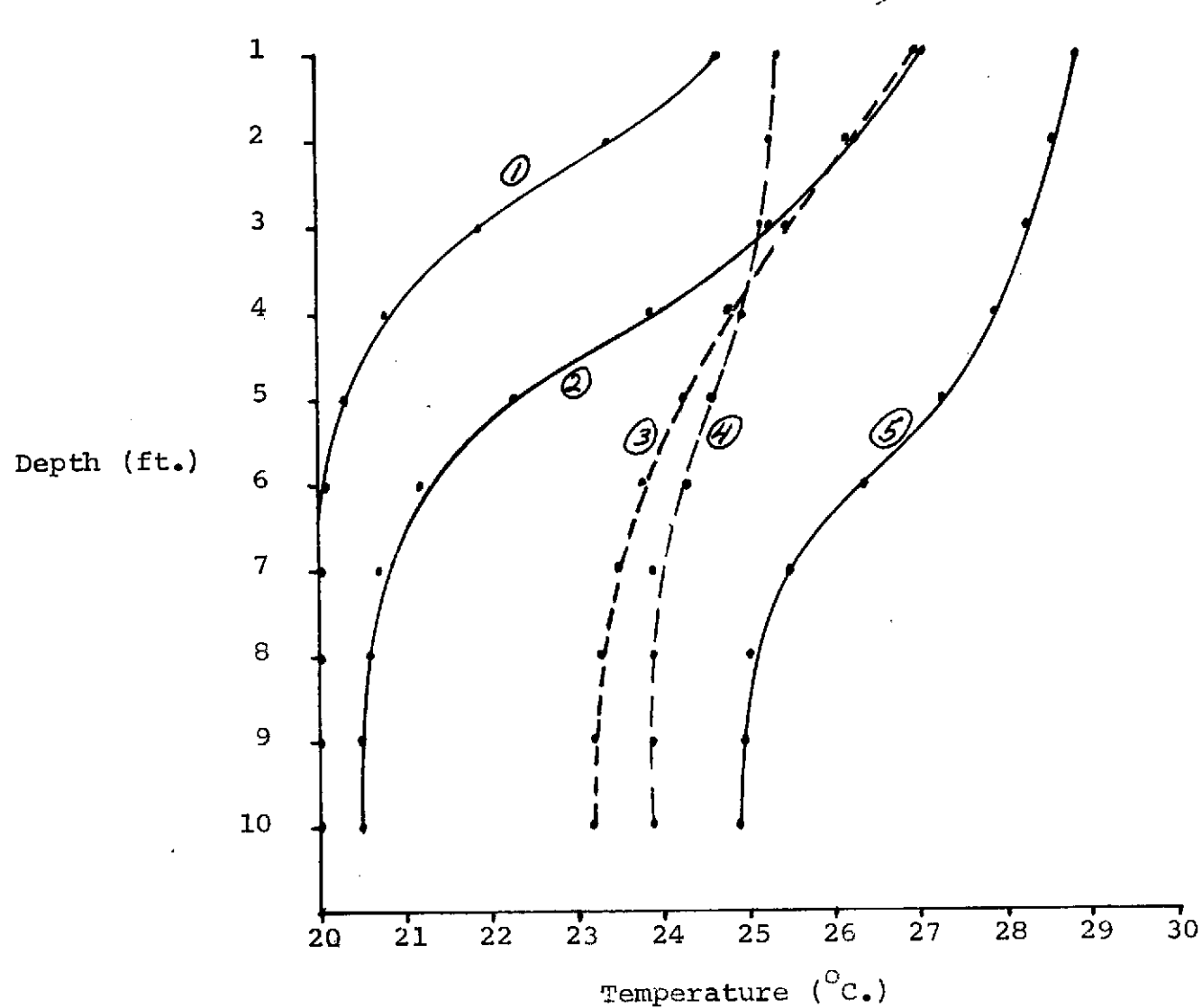


Figure 2.7 Flow Chart for Free-Surface Model



$$Kv = Kv_0 (1 + \sigma_1 Ri)^{-1}$$

$$Ri = \frac{\alpha_v g Z^2 \frac{\partial T}{\partial Z}}{W^2}$$

$Kv = 11.57$ cm/sec initially
for 1, 2 & 5, and constant
for 3.

Graphs:

1; Kv varies, 1 day

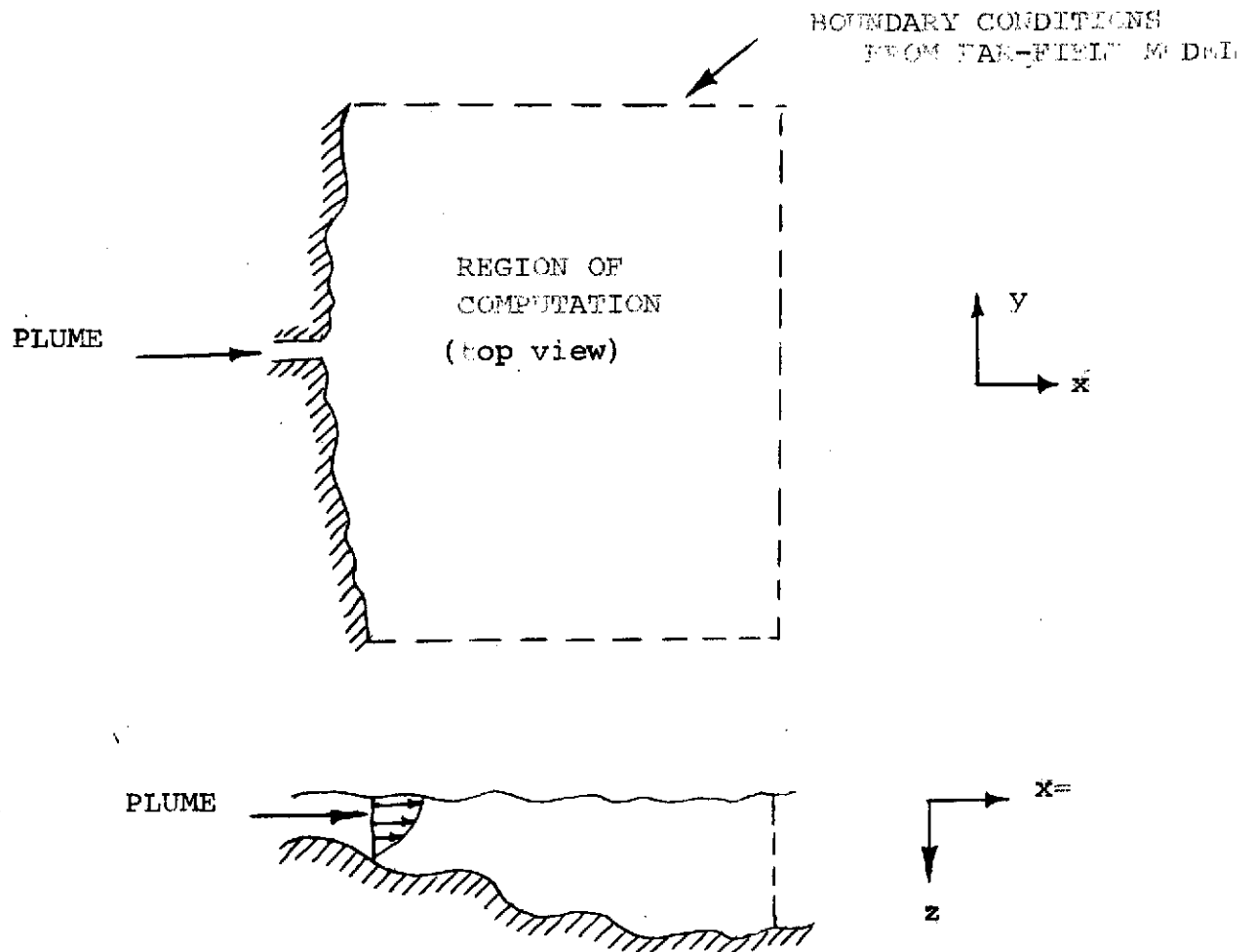
2; Kv varies, 5 days

3; Kv constant, 5 days

4; Biscayne Bay; data from
Feb. 18, 1972

5; Kv varies, 30 days

2.8 Vertical Temperature Profile; Typical Example



HORIZONTAL TRANSFORMATION

$$x = 1/c_1 \tan^{-1} (x/c_2)$$

$$y = 1/c_3 \tan^{-1} (y/c_4)$$

e.g. if $c_1 = \pi/2$ then $x = \alpha \Rightarrow X = 1.0$

Even increments in ΔX thus produce a close spacing of grid points near the plume entrance, where the best resolution is desired.

FIG. 2.9 NEAR FIELD MODEL

RECTANGULAR CONSTANT DEPTH APPROXIMATION

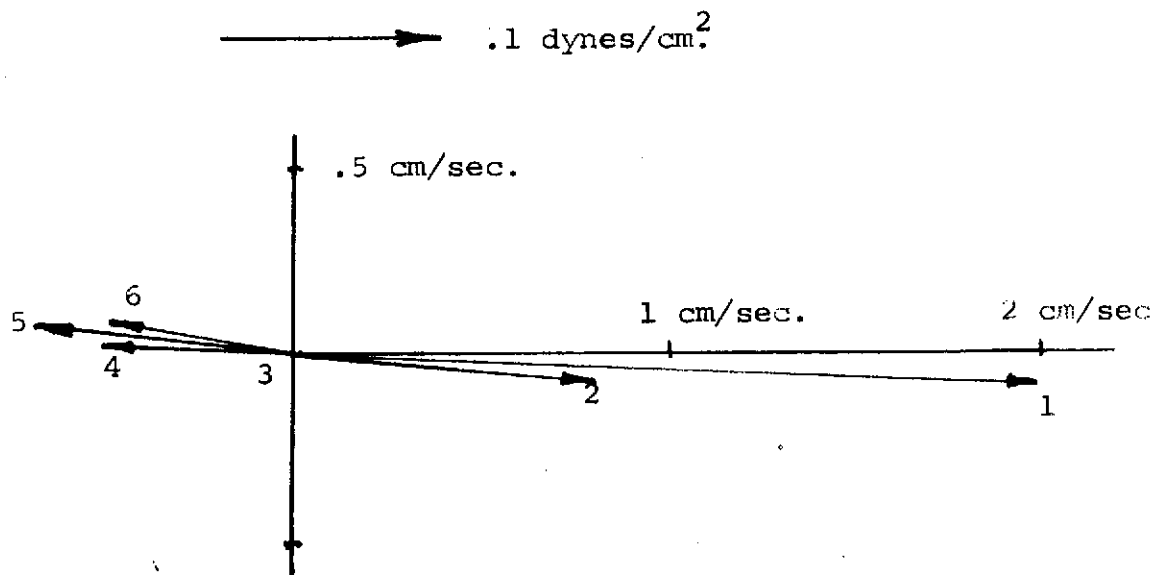
(25 km x 8 km x 4 m)

$\Delta x = \Delta y = 1 \text{ km}; \Delta z = 66.6 \text{ cm.}$

CASE-I

$$A_H = 10^4 \text{ cm}^2/\text{sec.}$$

$$A_V = 5 \text{ cm}^2/\text{sec.}$$



CASE-II

$$A_V = 1 \text{ cm}^2/\text{sec}; A_H = 10^4 \text{ cm}^2/\text{sec.}$$

REPRODUCIBILITY OF THE
ORIGINAL PAGE IS POOR

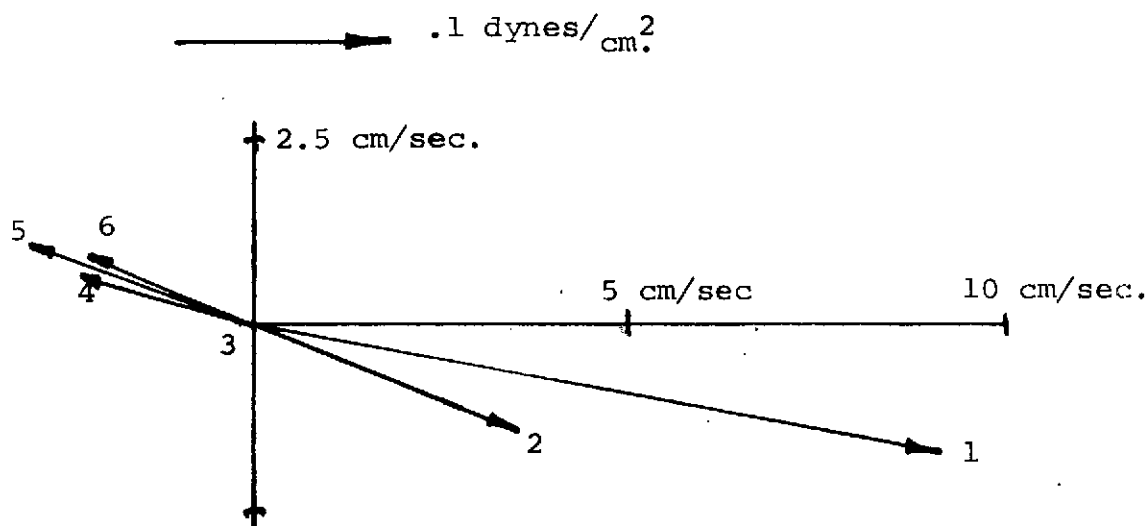
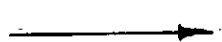


Figure 2-11 Velocity Profiles in Biscayne Bay; Constant Depth Approximation

Figure 2-12 Representative Parameters for Biscayne Bay

PARAMETER	EXPRESSION	SIGNIFICANCE	ESTIMATES * FOR BISCAYNE BAY
ASPECT RATIO	H/L	COMPARISON OF HORIZON- TAL AND VERTICAL SCALES	$.5 \times 10^{-3}$
Re; REYNOLDS NO.	$U_{ref} \cdot L / A_{ref}$	<u>INERTIA FORCES</u> VISCIOUS FORCES	800
R_B ROSSBY NO.	U_{ref} / fL	<u>INERTIA FORCES</u> CORIOLIS FORCES	.238
Pr PRANDTL NO.	A_{ref} / B_{ref}	<u>VISCOUS DIFFUSION</u> THERMAL DIFFUSION	1
Pe PECLET NO.	$\frac{U_{ref} \cdot L}{B_{ref}}$	Re.Pr. \sim <u>CONVECTION</u> DIFFUSION	800
Eu EULER NO.	$\frac{gH}{U_{ref}^2}$	<u>HYDROSTATIC PRESSURE</u> DYNAMIC PRESSURE	4000
Fr FRONDE NO.	$\frac{U_{ref}}{gH}$	SIMILAR TO EULER NUMBER	.0159
VISCOUS TIME SCALES	L^2 / A_H and H^2 / A_V	VERTICAL VISCOUS SCALE, HORIZONTAL VISCOUS SCALE	64×10^6 secs. and 32,000 secs
CONVECTIVE TIME SCALE	L / U_{ref}	TIME TAKEN FOR PARTICLE TO COVER LENGTH SCALE	80,000 secs.

* BASED ON L=8Km. $A_H=10,000 \text{ cm}^2/\text{sec}$, $A_V=5 \text{ cm}^2/\text{sec}$.
H=4M $f=.6 \times 10^{-4}/\text{sec}$.
 $U_{ref}=10 \text{ cm}/\text{sec}$.
 $A_{ref}=10,000 \text{ cm}^2/\text{sec}$; $B_{ref}=10,000 \text{ cm}^2/\text{sec}$.



Wind Stress = .1 dynes/cm²



.8 kilometers

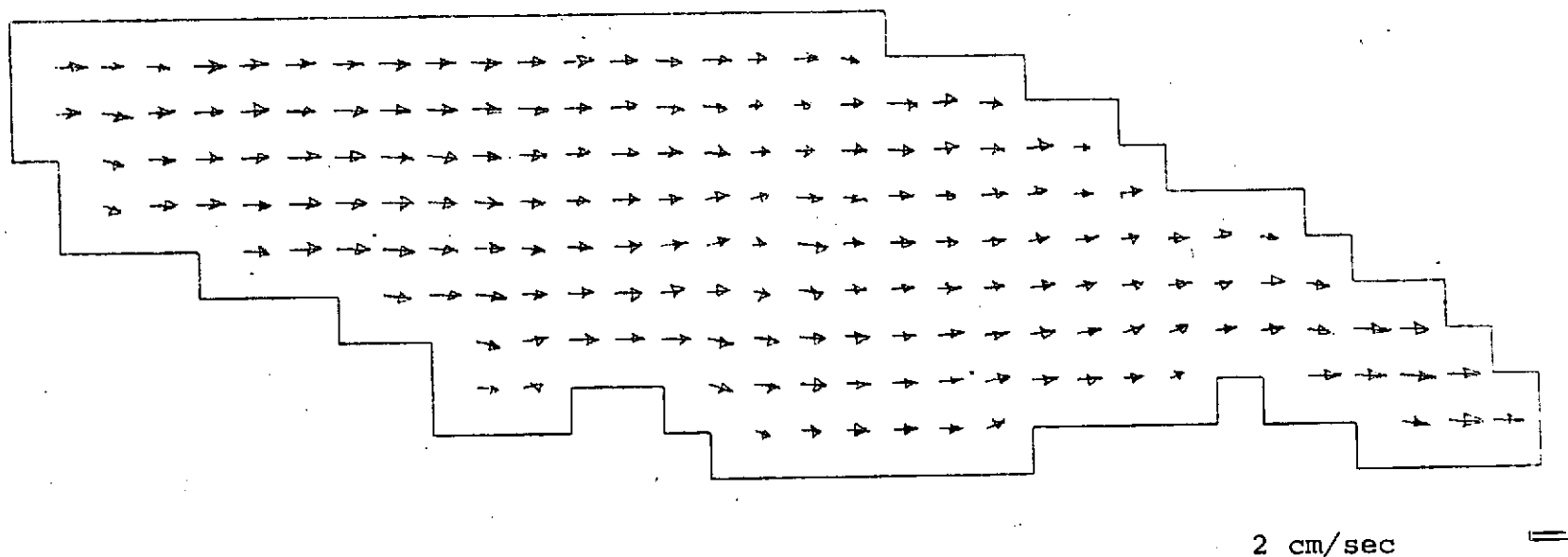
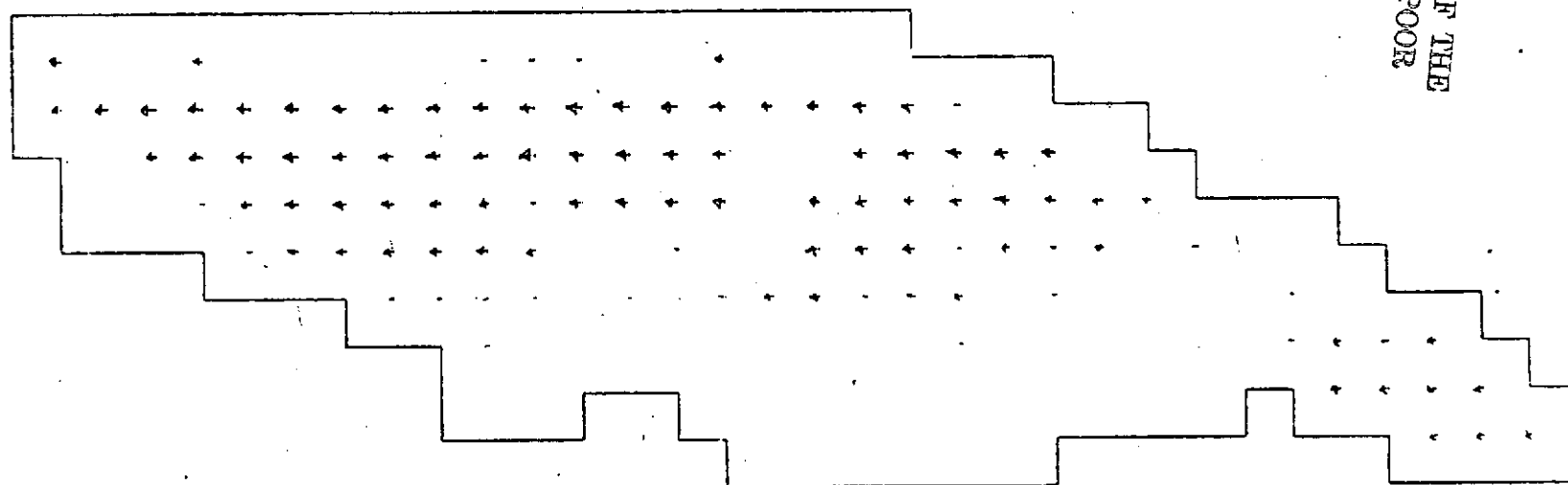


FIG. 2-13 Surface Velocities in Biscayne Bay with wind from the north

REPRODUCIBILITY OF THE
ORIGINAL PAGE IS POOR.

→
Wind Stress .1 dynes/cm²

— .8 Kilometers



2 cm/sec



2-14 Velocities at a depth of 2 meters with wind from the north

REPRODUCIBILITY OF THE
ORIGINAL PAGE IS POOR

Wind Stress = .1 dynes/cm²



.8 kilometers horizontal scale



3 ft. vertical scale

2 cm/sec

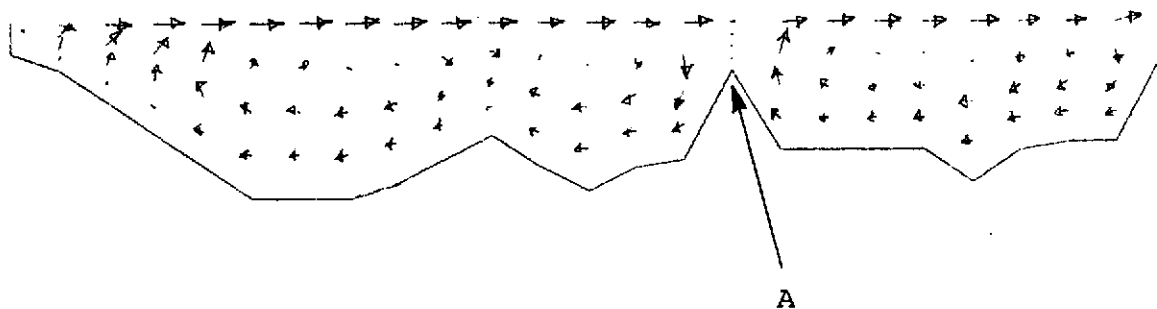
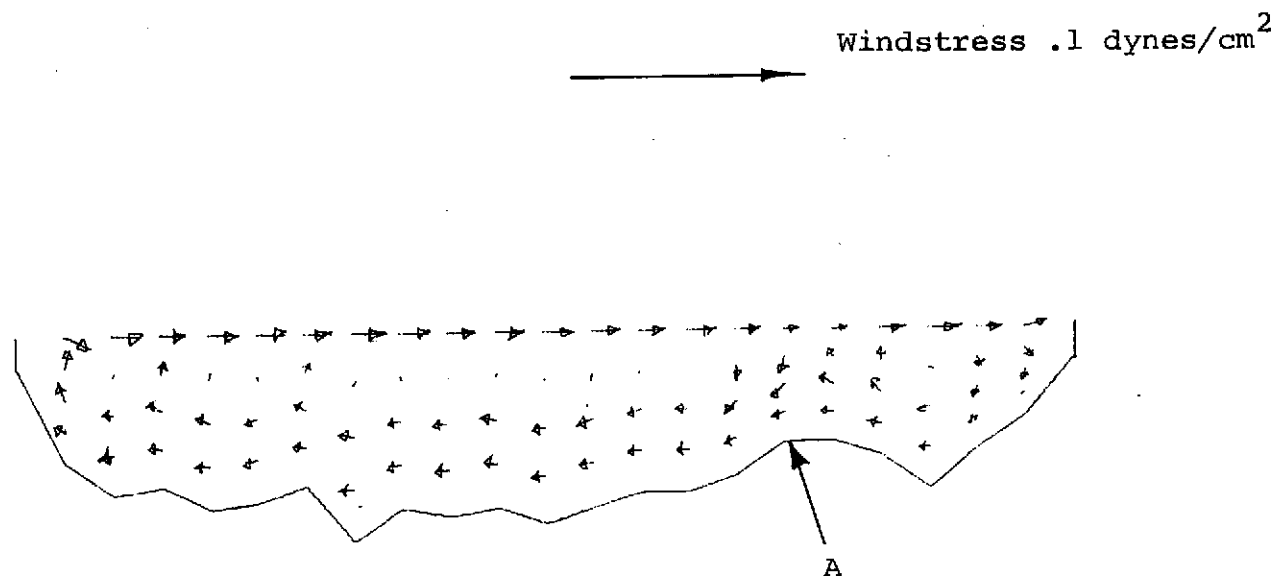


Figure 2-15 Velocities at section J = 7 with wind from the north

REPRODUCIBILITY OF THE
ORIGINAL PAGE IS POOR

□ .8 kilometers horizontal scale
□ 3 ft. vertical scale

□ 2 cm/sec



2-16 Velocities at section J = 9 with wind from the north

Wind Stress = .1 dynes/cm²

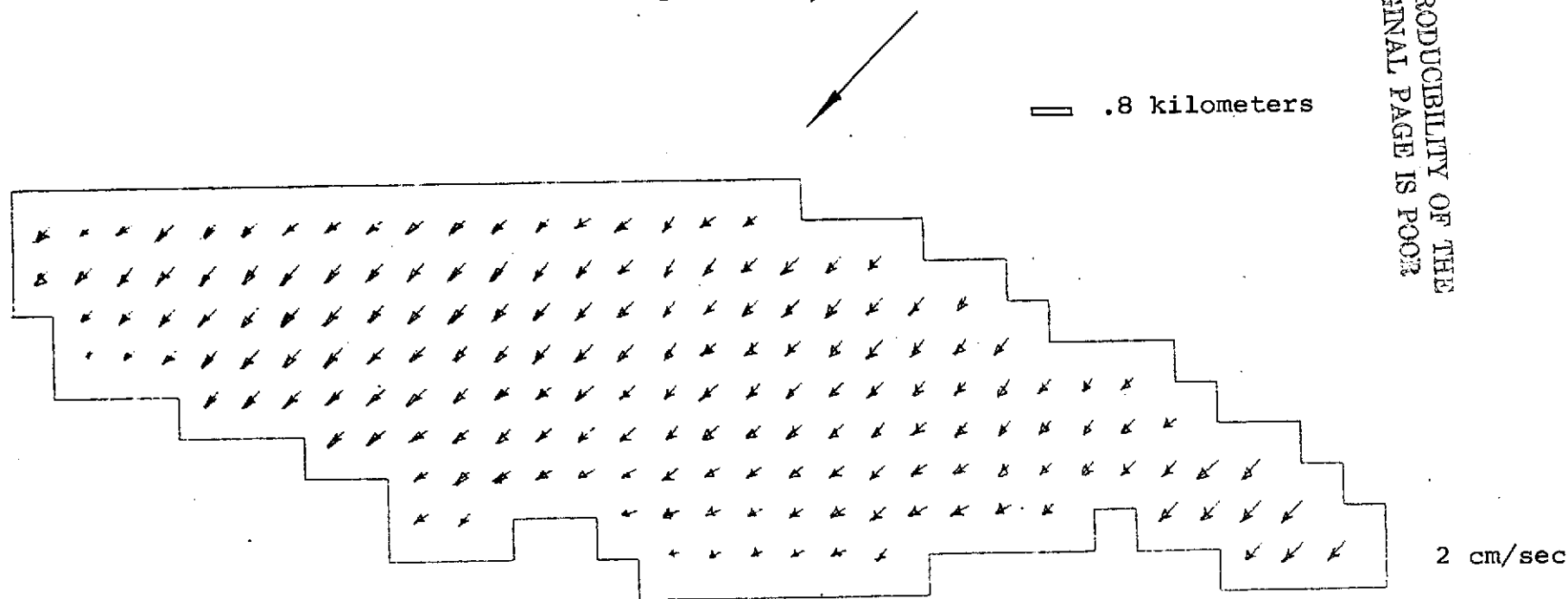


Figure 2-17 Surface Velocities with wind from southeast

REPRODUCIBILITY OF THE
ORIGINAL PAGE IS POOR

Wind Stress = .1 dynes/cm²

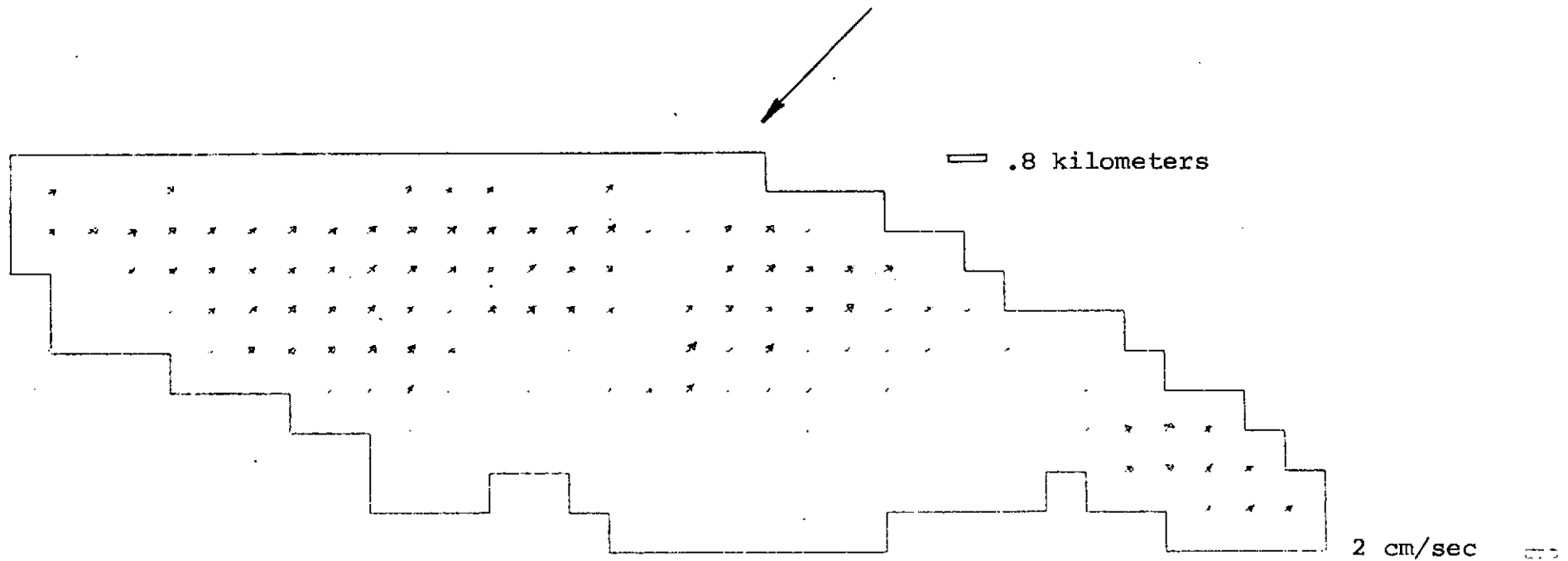


Figure 2-18 Velocities at a depth of 2 meters with wind from the Southeast

Wind Stress, 0.707 dynes/cm^2



□ .8 kilometers horizontal scale

3 ft. vertical scale

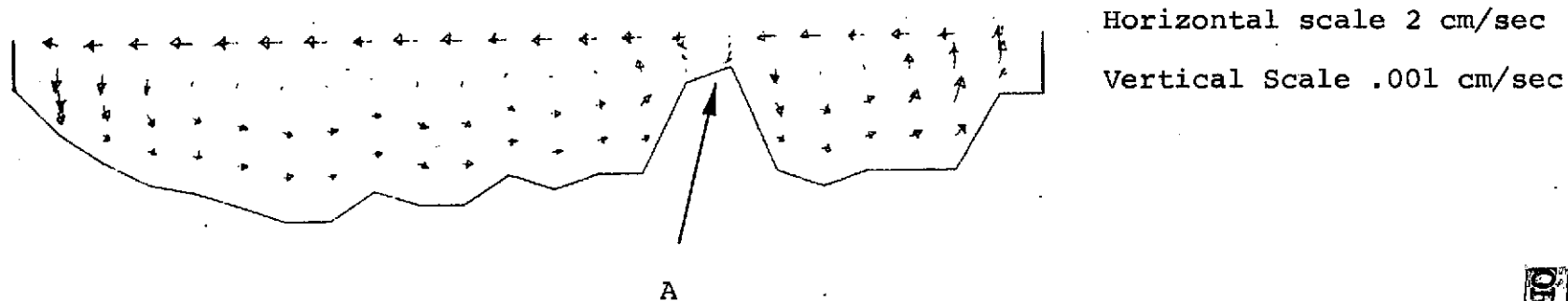


Figure 2-19 Velocities at section J = 8 with wind from the Southeast

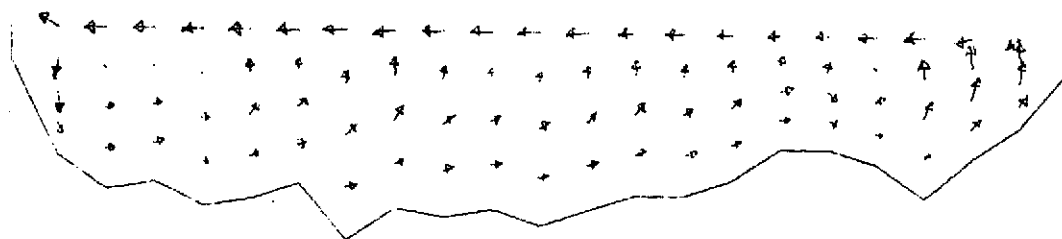
REPRODUCTION OF THE
ORIGINAL PAGE IS POOR

PRODUCIBILITY OF THE
ORIGINAL PAGE IS POOR

Wind Stress $.0707 \text{ dynes/cm}^2$

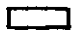


— .8 kilometers horizontal scale
3 ft. vertical scale



Horizontal scale 2 cm/sec
Vertical Scale .001 cm/sec

Figure 2-20 Velocities at section J = 9 with wind from the Southeast

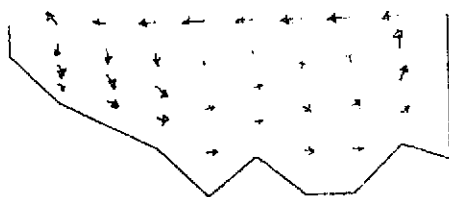

 .8 Kilometers horizontal scale
 3 ft. vertical scale

windstress = .0707 dynes/cm²



horizontal scale

2cm/sec. 



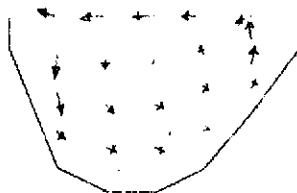
REPRODUCIBILITY OF THE
ORIGINAL PAGE IS POOR

windstress = .0707 dynes/cm²



horizontal scale

2cm/sec. 



vertical scale

.001 cm/sec.

Figure 2-21 Velocities at section I = 7 and I = 11 with wind from the Southeast.

REFERENCES

1. Ekman, V.X.: Uber Horizontal Cirkulation Winderzengten
2. Welander, P.: Wind Action on a Shallow Sea: Some Generalizations of Ekman's Theory. Tellus, Vol. 9, No. 1, February 1957.
3. Gedney, R. and W. Lick: Wind Driven Currents in Lake Erie. J.G.R. 77, 1972.
4. Bryan, K.: A Numerical Method for the Study of the World Ocean. J. Comp. Phys. 4, 1969.
5. Crowley, W.P.: A Global Numerical Ocean Model: Part I. J. Comp. Phys. 3, 1968.
6. Crowley, W.P.: A Numerical Model for Viscous Free Surface Barotropic Wind-Driven Ocean Circulation. J. Comp. Phys., 5, 1969.
7. Crowley, W.P.: A Numerical Model for Viscous Non-Divergent, Barotropic, Wind-Driven, Ocean Circulations. J. Comp. Phys. 6, 1970.
8. Berdahl, P.: Oceanic Rossby Waves: A Numerical Rigid-Lid Model. ITD-4500, UC034. Lawrence Radiation Laboratory, University of California, Livermore. 1969.
9. Sengupta, S. and Lick, W.: A Numerical Model for Wind Driven Circulation and Temperature Fields in Lakes and Ponds. FTAS TR. 74/95. Case Western Reserve University, 1974.
10. Phillips, N.A.: A Co-ordinate System Having Some Special Advantages for Numerical Forecasting. J. Meteorol., 14, 1957
11. Freeman, N.G., Hale, A.M., Damard, M.B.: A Modified Sigma Equations Approach to the Numerical Modeling of Great Lakes Hydrodynamics. J. Geo. Res., Vol. 77, No. 6, 1972.
12. Dean, R.A., et al.: Numerical Modeling of Hydromechanisms of Biscayne Bay/Card Sound System, Part I: Non-Dispersive Characteristics, University of Florida, Coastal Engineering Department Report. 1971.
13. Policastro, A.J. and Tokar, J.V.: Heated-Effluent Dispersion in Large Lakes. State of the Art of Analytical Modeling. Part I Critique of Model Formulations. Report No. ANL/ES-11, Argonne National Laboratory, Argonne, Illinois. 1972.

14. Policastro, A.J.: Heated Effluent Dispersion in Large Lakes. State-of-the Art of Analytical Modeling, Surface and Submerged Discharges. Presented at the Topical Conference, Water Quality Considerations. Siting and Operating of Nuclear Power Plants, Atomic Industrial Forum, Inc., 1-4 October 1972.
15. Policastro, A.J. and R.A. Paddock: Analytical Modeling of Heated Surface Discharges with Comparisons to Experimental Data. Interim Report No. 1. Presented at the 1972 Annual Meeting of the A.I.Ch.E., 26-30 November, 1972.
16. Paul, J.F. and Lick, W.J.: A Numerical Model for a Three-Dimensional, Variable-Density Jet. FTAS/TR7392 School of Engineering, Case Western Reserve University. 1972.
17. Waldrop, W.R., and Farmer, R.C.: Three-Dimensional Computation of Buoyant Plumes. J.G.R. Vol 79, No. 9, 1974.
18. Rooth, C., and Lee, T.N.: A Method of Estimating Thermal Anomaly Areas from Hot Discharges in Estuaries, Sea Grant Bulletin No. 3, University of Miami, 1970.
19. Haq, A. and Lick, W.: The Time-Dependent Wind-Driven Flow in a Constant Depth Lake, presented at the 16th Conference on Great Lakes Research, Huron, Ohio, 1973.
20. Hirt, C.W. and Harlow, F.H.: A General Corrective Procedure for the Numerical Solution of Initial-Value Problems, J. Comp. Phys. 2, 1967.
21. Edinger, J.E. and Geyer, J.C.: Heat Exchange in the Environment, E.E.I. Publication, No. 65-902, Edison Electric Institute, 1971.
22. Munk, W.H. and Anderson, E.R.: Notes on a Theory of the Thermocline, Journal of Marine Research, Vol. 7, 1948.
23. Sunderam, T.R. and Rehm, R.G.: Formation and Maintenance of Thermoclines in Stratified Lakes Including the Effects of Power-Plant Thermal Discharges. AIAA Paper No. 70-238, 1970.
24. Dake, J.M. K. and Harlemann, D.R.F.: Thermal Stratification in Lakes: Analytical and Laboratory Studies, Water Resources Research, Vol. 5, No. 2, 1969.

III. GROUND TRUTH & IN-SITU MEASUREMENTS

A. OBJECTIVE

The major functions of the measurements in this portion of the project are to provide:

- 1) Ground truth data for calibration and verification of the remotely sensed measurements.
- 2) Boundary conditions and physical constants of the areas investigated for the mathematical model.
- 3) Assistance in the development of new remote sensing techniques.

The measurements can also prove useful in determining the validity of the model as the predictions based on it can be confirmed by future measurements under the assumed conditions.

The quantities of interest in the measurement program are:

- 1) surface temperature
- 2) temperatures at intermediate depths and at the bottom
- 3) current speed and direction
- 4) salinity
- 5) turbidity
- 6) pertinent meteorological data such as atmospheric temperature, wind speed, wind direction, and humidity.

Surface temperatures are measured both by direct means and by an infrared radiation type instrument. The major use of the surface temperature measurements is for the calibration of the remotely-sensed temperature. The direct measurements are obtained with an accurate thermometer and with a thermistor at several depths very close to the surface; the latter to detect any possible temperature gradient close to the surface. Due to possible shifts in the calibration, it was found that a single thermistor moved to the several depths is preferable to the use of several thermistors so that comparative readings will be meaningful.

The other quantities listed in the measurement program above are primarily intended for the model studies. The temperature profiles are needed to determine the vertical temperature gradients and will be obtained at several horizontal locations for the three dimensional information. Current flows at several of the inlet areas of the bay are also of importance to the model study. Salinity and turbidity measurements are of secondary interest but will be done as conditions permit. The meteorological data has proven useful both for the model studies and for the remote sensing of the surface temperature.

B. MEASUREMENT SYSTEM

The instruments used in this program are listed in Table 3-1. The thermistors are standard 4000 ohm semiconductors whose resistance is a function of the temperature. Calibration curves for the thermistors used are shown in Figs. 3-1, 3-2, 3-3, and 3-4. These curves were obtained using a temperature bath control, and the resistance was measured by a L & N Wheatstone Bridge. Unfortunately, the bridge's internal batteries resulted in an excessively high voltage across the thermistor causing resistance changes due to ohmic heating. Instead an external 1.5 volt dry cell is used which limits the thermistor dissipation to under 1 milliwatt,

eliminating this problem. Although this reduces the sensitivity of the bridge, the readings within the nearest 10 ohms are nevertheless consistent with the accuracy and stability of the calibrations and sensors. Another problem has been reading the bridge galvanometer on board the vessel during tests because of the boat motion. A digital null device with amplification is presently under consideration to eliminate this difficulty.

The "Heat Spy" has not given consistent readings within its nominal accuracy and the reason is under investigation. During the run of August 21, it apparently had satisfactory results, but in some preliminary tests its performance was questionable. The problem appears to be a leakage of radiation through the shutter. A "black body" apparatus has been fabricated to calibrate this device. The flowmeter used is of the rotor type which is most suitable for the low currents and shallow depths of Biscayne Bay. The manufacturer, General Oceanics, which is based in Miami, modified their read-out system so that an audible "beep" is heard for every half revolution. This has proven invaluable in obtaining an average flow since the number of revolutions for an extended period can be determined, thus providing an integrated output. When measuring the current of the Hutchinson River Island installation an inclinometer type instrument with direction indication and a depth sensor will be used since the flows will be greater and measurements will have to be made in deeper water.

The Turbidimeter was calibrated against a laboratory type instrument and the results are shown in Fig. 3-5. The transmissivity indicated by this meter, however, does not appear to be a good measure of the clarity of the water in terms of the water appearance. The salinity bridge was completely unsatisfactory as the readings were absurd. The reason is under investigation and it may be necessary to employ a higher quality conductivity meter in the future if this information is deemed desirable. The other instruments are routine and need not be discussed.

C. PROCEDURES

The procedure for shipboard tests followed established practice for this type of activity. The operation of each instrument was verified in the laboratory and then stored in the instrument carrying case using a checklist for all equipment and accessories. On board, the instruments were unpacked during departure and readies for use. In the tests made in conjunction with the NASA-6 aircraft, the surface temperature measurements were stressed, and consequently, readings at lower depths were eliminated since they would consume valuable time. For this type of test, it is of greater importance to make as many surface measurements as possible at as many sites as possible since the objective is to correlate the ground truth and remote measurements.

In the runs made for acquiring three-dimensional data for the model studies, temperatures and current flows were obtained at several depths, mainly at inlet areas of the Bay. Prior to departure, responsibilities for the various measurements were assigned to the individual members of the staff, and each investigator noted and recorded his particular measurements. While underway to the next station, the data was entered on the forms provided for this purpose. Certain readings such as the resistances of the thermistors were converted to temperatures so that discrepancies could be noted immediately. The current speed was also converted to its value in cm. per sec. using the relation that two "beeps" correspond to 1 revolution and that one cycle per sec. (Hertz) corresponds to 50 cm. per sec. for the impeller blade used. Other readings were direct. In the final data sheets, all temperatures were recorded in degrees centigrade since most of the instruments are calibrated in this unit.

D. RESULTS AND DISCUSSION

The data sheets for the tests of July 29, 1974 and August 21, 1974 are shown in Tables 3-2 and 3-10. It should be emphasized here that these tests were trial runs to establish procedures, test the instruments, and try to correct problem areas. In the July 29th tests, there were sharp disagreements between the temperatures obtained by the thermistors at the 1½" depth and the 5" depth. Two separate thermistors were used, and, due to changes in their characteristics, yielded these faulty readings. The procedure has been modified so that only one thermistor is used for both depths and this sensor is re-calibrated soon after the completion of the shipboard tests for the temperature range used. Using the same thermistor, comparative readings would be valid, and careful recalibration would ensure the absolute readings. This procedure was followed during the tests of August 21st and it resulted in more meaningful information. The major problem area for the thermistor measurements is the difficulty of reading the galvanometer on the ship. Since an indication of the bridge balance is the objective rather than a specific deflection, a polarity indicator (digital) would suffice. It is hoped to have a unit fabricated within the next few months with sufficient amplification for proper sensitivity. If the model studies deem it necessary, an improved conductivity indicator will be obtained for more meaningful salinity measurements. The other measurements seem to be satisfactory and no changes are presently contemplated.

From the trial runs and the experience acquired in the use of the instruments, future experimental efforts should be more fruitful. Procedures have been established, and all personnel have been trained in the operation of all the instruments. This is the significant conclusion since the bulk of the experimental portion of the project lies ahead.

Resistance, Kilo-ohms

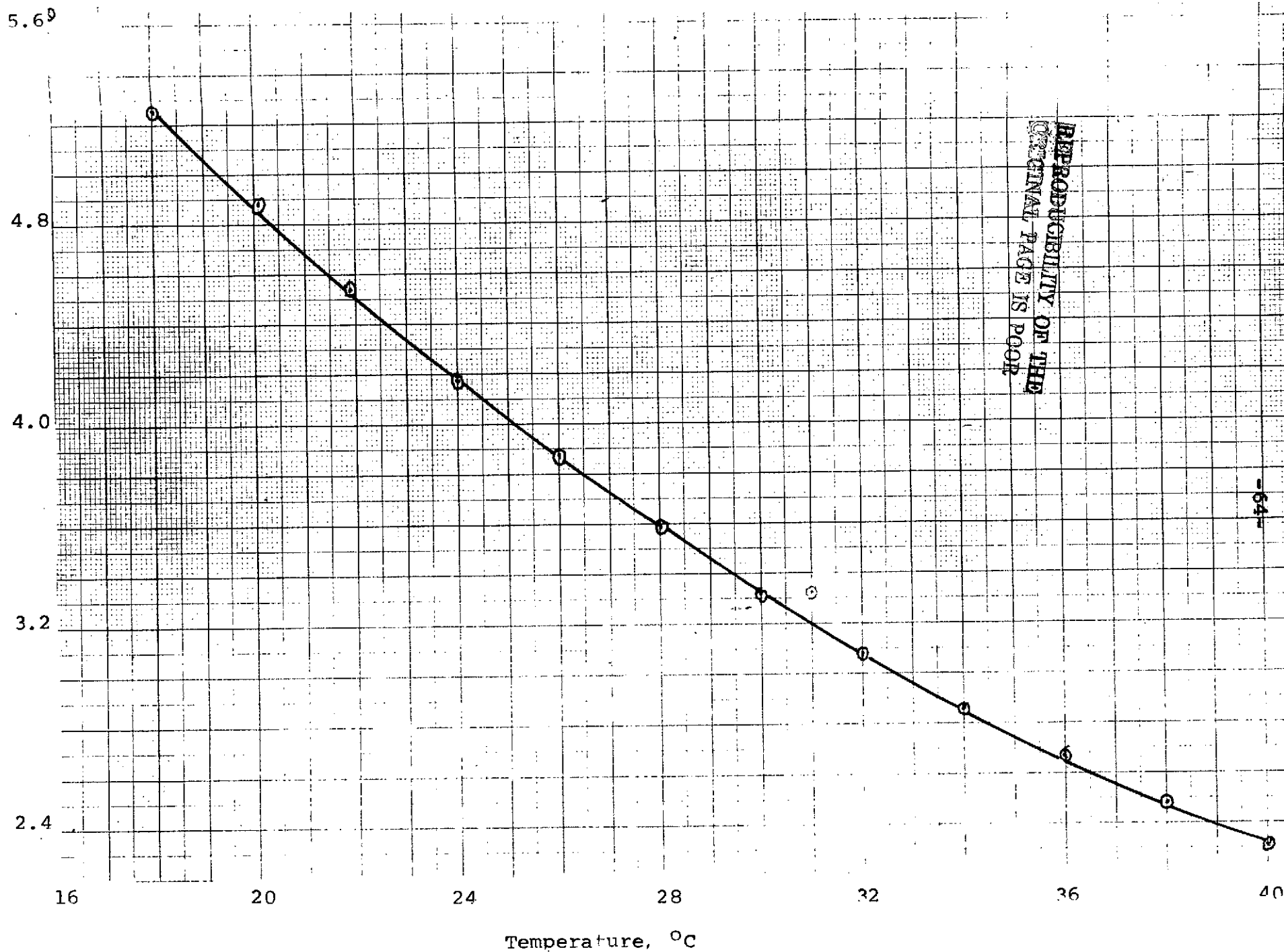


Fig. 3-1 Calibration Curve for H-21 Thermistor (Open Case)

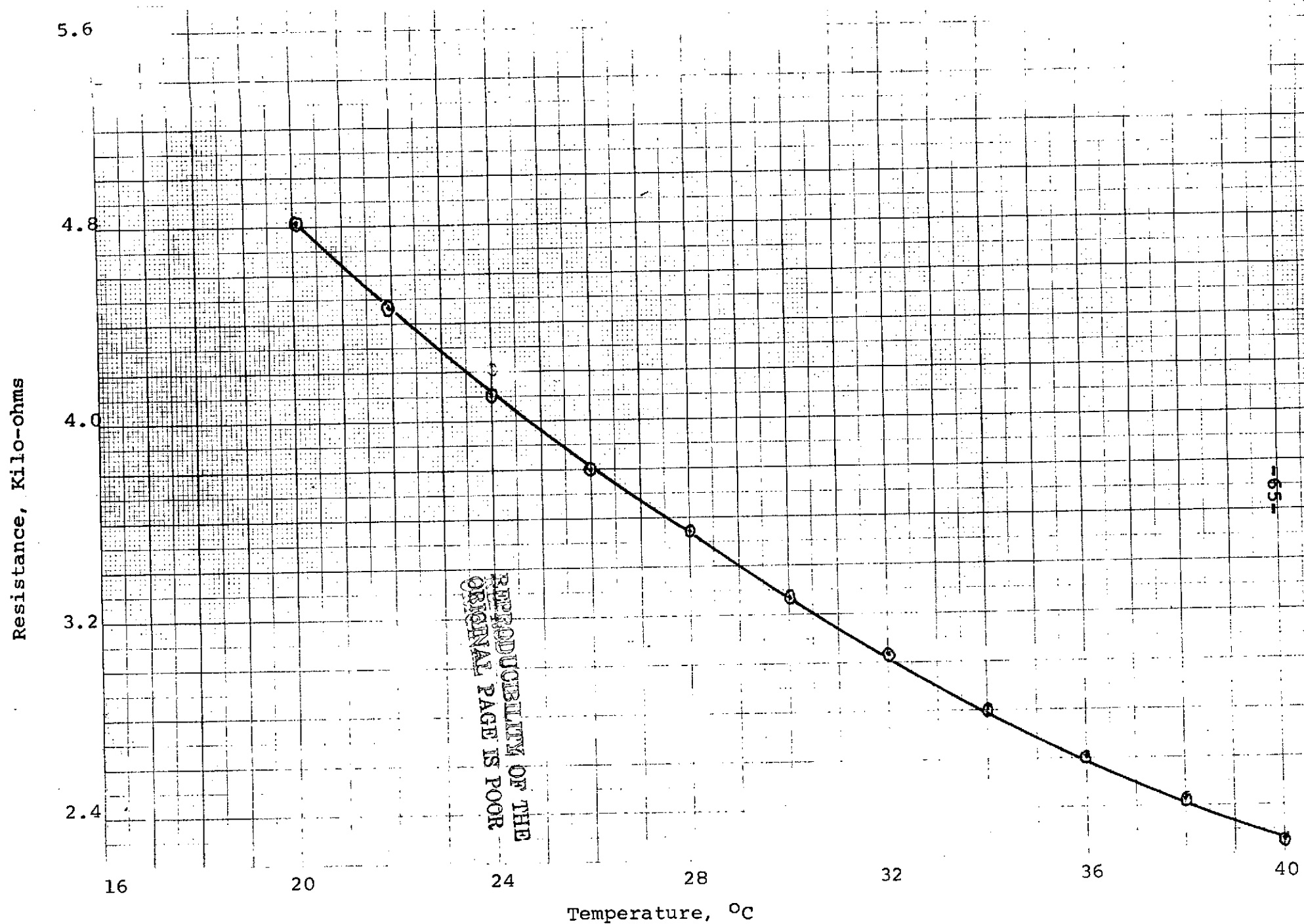


Fig. 3-2 Calibration Curve for K-805 Thermistor

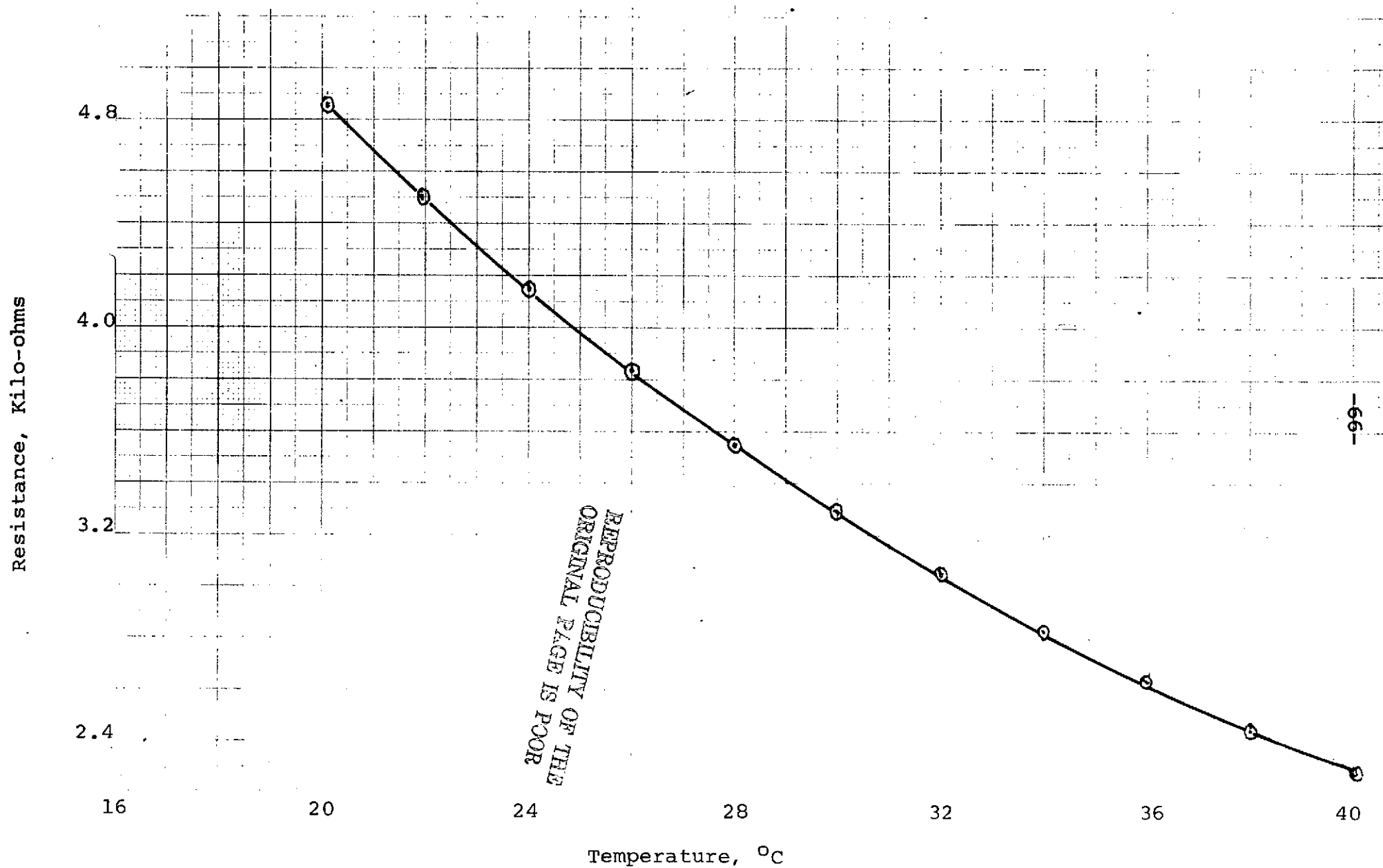


Fig. 3-3 Calibration Curve for K-3007 Thermistor - Unit No. 1

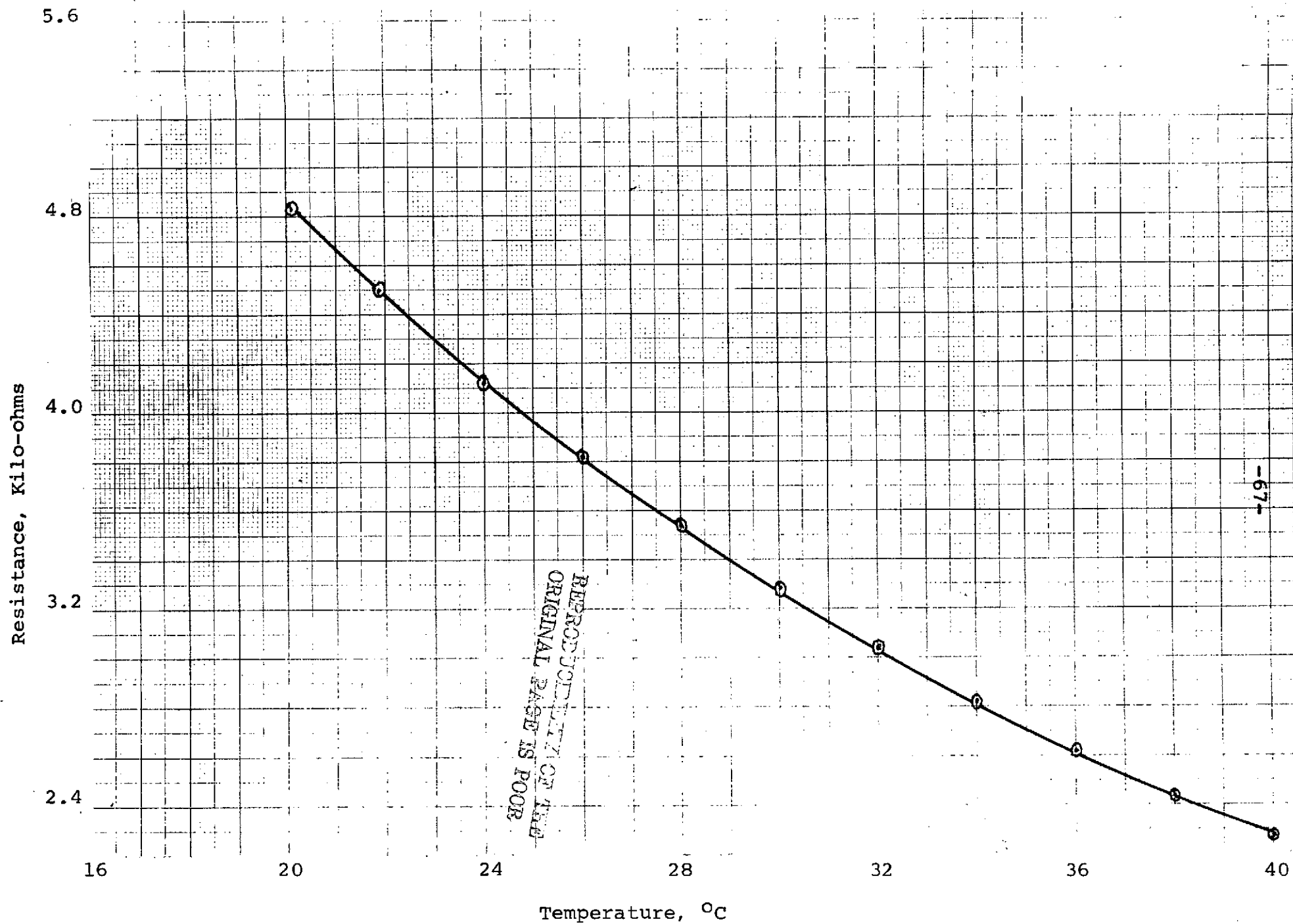


Fig. 3-4 Calibration Curve for K-3007 Thermistor - Unit No. 2

Fig. 3-5 Calibration Curve
for Beckman EV-4
Using Hach Model 2100A
Turbiditimeter # 1300

FTU are Formazin
Turbidity Units

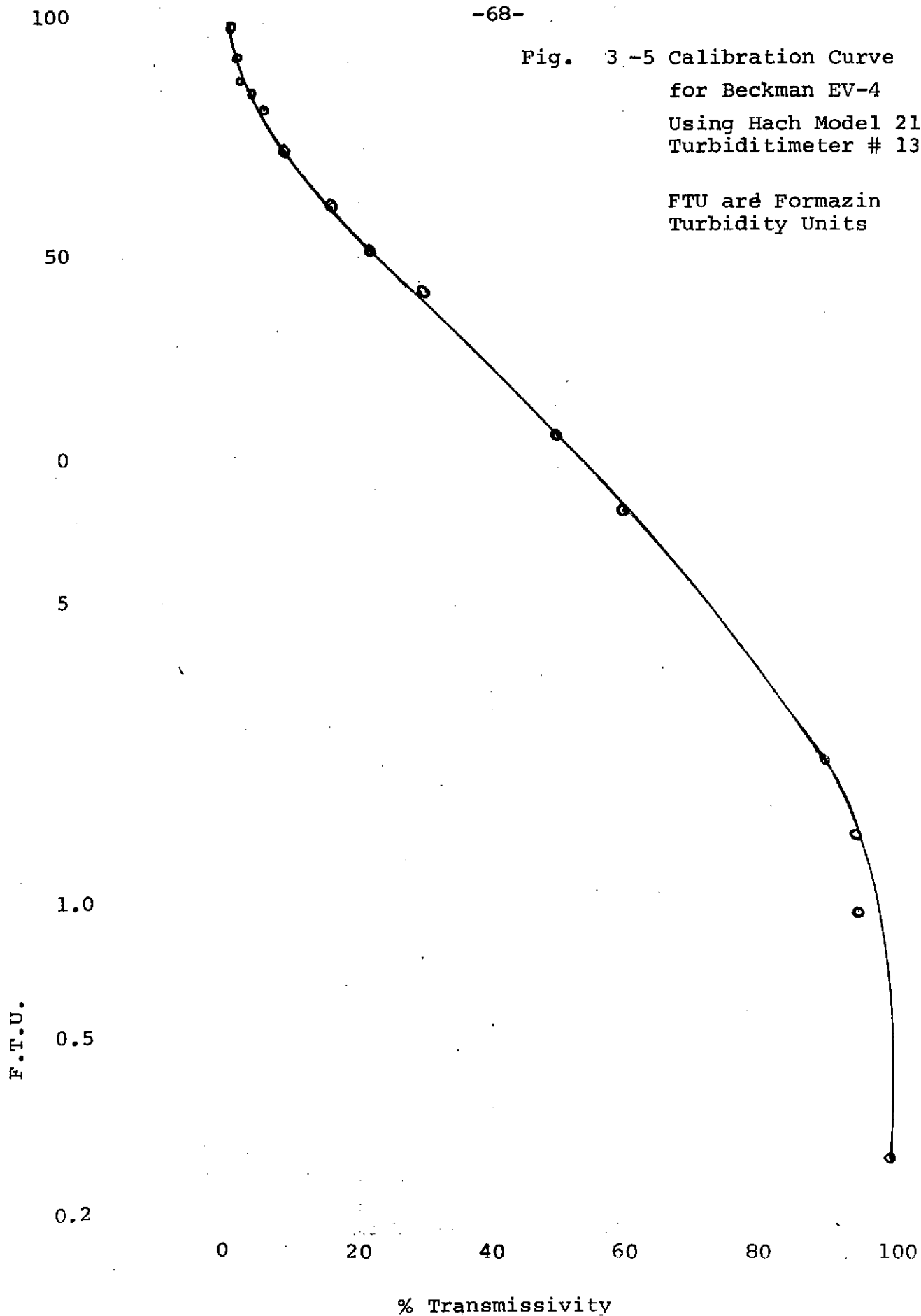


TABLE 3-1

List of Equipment

<u>Equipment</u>	<u>Planned Use</u>	<u>Sensitivity</u>
1) Fenwal Thermistors 2 H66 GB34J92 1 H21 GB34J92	Sensor for Measurement of Temperature	.05°C at 30°C
2) "Circu-Temp" Precise Bath Temperature Control "Temp-Tact" Thermoregulator Model A	Temperature Source for Calibration of Thermistors	0.1°C
3) Deluxe Marine Sextant Catalog #742 Edmund Scientific Corp.	Determine Location	± 1 minute of arc
4) Model HSA-1G Heat Spy Automatic Infra-red Thermometer Wahl Corp., L.A., Calif.	Infra-red Detection of Temperature	± .1°C
5) Leeds & Northrup Model 5305 Type S-1 Resistance Bridge	Measurement of the Resistance of the Thermistors	.15% Approx. 6 ohms for Thermistors
6) General Oceanics Model 2031 Digital Flowmeter & Model 2035 Flowmeter Deck Readout	Measurement of Current Flow	Minimum flow approx. ½ cm./sec.
7) Bechman Environline Model EV-4 Underwater Turbidimeter	Measurement of Turbidity	Approx. ± 2½% Transmissivity
8) Beckman Salinity Temperature Bridge	Measurement of Salinity	± 1 part per thousand 0-40 ppt.
9) 4" Biram Type Anemometer Davis Instrument Co.	Wind Velocity	± 1 foot per minute
10) Sling Psychrometer Bacharach Industrial Instrument Co.	Relative Humidity Air Temp.	± ½°F ± ½% humidity

TABLE 3-2

REMOTE SENSING DATA SHEET

Date 7/29/74

Station: #1 (Near Shore) Lat. 25° 35.217'
Long. 80° 16.845'

Time: 8:00 AM

Air Temperature: 28° C

Humidity: 77%

Wind Speed: 600 ft. per min.

Sea State: calm

Wind Direction: S.W.

Sky Condition: clear, high cloud

Depth:

Infrared Surface Temperature: 26.6°C

	Near Surface Depth: 1½"	Depth: 5"	2/3 Depth From Surface Depth:	Near Bottom Depth:
Thermistor Readings in ohms	3020 ohms 32.5°C	3410 ohms 28.9°C		
Thermometer Reading	29°C			
Current cm/sec Current Dir.	1.4cm./sec. 240° (Magnet from N)			
Turbidity (Trans- mittance, %)	90%			
Sal. Bridge				
Salinity:				
Temperature:				

REPRODUCIBILITY OF THE
ORIGINAL PAGE IS POOR

REMARKS: Data taken in conjunction with NASA-6 Aircraft. Average of readings indicated here first position on eastward run.
H-21 Thermistor used for 1½" depth
K805 Thermistor used for 5" depth

TABLE 3-3

REMOTE SENSING DATA SHEET

Date 7/29/74

Station: #7 Lat. $25^{\circ}35.283'$
Long. $80^{\circ}13.571'$

Time: 8:55AM

Air Temperature: 29°C

Humidity: 76%

Wind Speed: 789 ft. per min.

Sea State: calm

Wind Direction: 225° (magnet from N.)

Sky Condition: clear, high cloud

Depth:

Infrared Surface Temperature: 28.3°C

	Near Surface		2/3 Depth From	Near Bottom
	Depth: $1\frac{1}{2}"$	Depth: 5"	Surface	Depth:
Thermistor Readings in ohms	2710 ohms 35.3°C	3200 ohms 30.5°C		
Thermometer Reading	31°C			
Current cm/sec Current Dir.	13.8cm/sec. 235° (from N)			
Turbidity (Trans- mittance, %)	90%			
Sal. Bridge:				
Salinity:				
Temperature:				

REPRODUCTION OF THIS
ORIGINAL PAGE IS FORBIDDEN

Remarks: Data taken in conjunction with NASA-6 Aircraft. Average of readings indicated here; second position on eastward run.
H-21 Thermistor used for $1\frac{1}{2}"$ depth
K805 Thermistor used for 5" depth

TABLE 3-4

REMOTE SENSING DATA SHEET

Date 7/29/74

Station: #12(Near Soldier Key) Lat.25°35.348'
Long.80°10.875'

Time: 9:30AM

Air Temperature: 29°C

Humidity: 75%

Wind Speed: 735 Ft. per min.

Sea State: calm

Wind Direction: 255° (from N.)

Sky Condition: clear, high cloud

Depth:

Infrared Surface Temperature: 28.3°C

	Near Surface		2/3 Depth From Surface	Near Bottom
	Depth: 1½"	Depth: 5"	Depth:	Depth:
Thermistor Readings in ohms	2720 ohms 35.2°C	3280 ohms 29.9°C		
Thermometer Reading	30°C			
Current cm/sec Current Dir.	27.1 cm/sec. 260° (from N)			
Turbidity (Transmittance,%)	90%			
Sal. Bridge				
Salinity:				
Temperature:				

Remarks: Data taken in conjunction with HASA-6 Aircraft . Average of readings indicated here; third position on eastward run.
H-21 Thermistor used for 1½" depth
K805 Thermistor used for 5" depth

TABLE 3-5

REMOTE SENSING DATA SHEET

Date 7/29/74

Station: #12(Near Soldier Key) Lat. $25^{\circ}35.348'$
Long. $80^{\circ}10.875'$

Time: 10:30AM

Air Temperature: 31°C

Humidity: 69%

Wind Speed: 857 ft. per min.

Sea State: calm

Wind Direction: 215° (from N.)

Sky Condition: clear, high cloud

Depth:

Infrared Surface Temperature: 28.3°C

	Near Surface Depth: $1\frac{1}{2}"$	Depth: 5"	2/3 Depth From Surface Depth:	Near Bottom Depth:
Thermistor Readings in ohms	2820 ohms 34.3°C	3190 ohms 30.6°C		
Thermometer Reading	30°C			
Current cm/sec Current Dir.	28.3 cm/sec. 250° (from N)			
Turbidity (Trans- mittance, %)	90%			
Sal. Bridge				
Salinity:				
Temperature:				

REMARKS: Data taken in conjunction with NASA-6 Aircraft. Average of readings indicated here; first position on westward run.

H-21 Thermistor used for $1\frac{1}{2}"$ depth

K805 Thermistor used for 5" depth

REMOTE SENSING DATA SHEET

Date 7/29/74Station: #7(Near Buoy) Lat.25°35.283'
Long.80°13.571'

Time: 11:10AM

Air Temperature: 30°C

Humidity: 70%

Wind Speed: 1132 ft. per min.

Sea State: choppy

Wind Direction: 180° (from N.)

Sky Condition: Raining

Depth:

Infrared Surface Temperature: 29.4°C

	Near Surface		2, 3 Depth From	Near Bottom
	Depth: 1½"	Depth: 5"	Surface	Depth:
Thermistor Readings in ohms	2710 ohms 35.3°C	3160 ohms 30.8°C	Depth:	
Thermometer Reading	31°C			
Current cm/sec Current Dir.	24.6 cm/sec 210°(from N)			
Turbidity (Trans- mittance,%)	90%			
Sal. Bridge:				
Salinity:				
Temperature:				

REPRODUCIBILITY OF THE
ORIGINAL PAGE IS POOR

Remarks: data taken in conjunction with NASA-6 Aircraft. Average of readings indicated here; second position on westward run.
H-21 Thermistor used for 1½" depth
K805 Thermistor used for 5" depth

REMOTE SENSING DATA SHEET

Date 7/29/74

Station: #1(Near Shore) Lat. $25^{\circ}35.217'$
Long. $80^{\circ}16.845'$

Time: 12:00 Noon

Air Temperature: 27°C

Humidity: 74%

Wind Speed: 707 ft. per min.

Sea State: calm

Wind Direction: 235° (from N.)

Sky Condition: partly cloudy

Depth:

Infrared Surface Temperature: 28.9°C

	Near Surface		2/3 Depth From	Near Bottom
	Depth: $1\frac{1}{2}"$	Depth: 5"	Surface	Depth:
	Depth:	Depth:	Depth:	Depth:
Thermistor Readings in ohms	2840 ohms 34.1°C	3200 ohms 30.5°C		
Thermometer Reading	30°C			
Current cm/sec Current Dir.	25.1 cm/sec 195° (from N)			
Turbidity (Trans- mittance,%)	97%	REPRODUCIBILITY OF THE ORIGINAL PAGE IS POOR		
Sal. Bridge:				
Salinity:				
Temperature:				

Remarks: Data taken in conjunction with NASA-6 Aircraft. Average of readings indicated here; third position on westward run.

H-21 Thermistor used for $1\frac{1}{2}"$ depth

K805 Thermistor used for 5" depth

TABLE 3-8

REMOTE SENSING DATA SHEET

Date 8/21/74

Station: A Lat. $25^{\circ}41.39'$
Long. $80^{\circ}12.86'$

Time: 9:40AM

Air Temperature: 30°C

Humidity: 74%

Wind Speed: 660 ft. per min.

Sea State: Light chop

Wind Direction: 135° (from N)

Sky Condition: High broken clouds
30% low clouds

Depth: 12 ft.

Infrared Surface Temperature: 30.5°C

	Near Surface Depth: 1 ft.	1/3 Depth From Surface Depth: 4 ft.	2/3 Depth From Surface Depth: 8 ft.	Near Bottom Depth: 12 ft.
Thermistor Readings in ohms	3170 ohms 30.7°C	3180 ohms 30.7°C	3180 ohms 30.7°C	3190 ohms 30.6°C
Thermometer Reading	31.0°C			
Current cm/sec Current Dir.	5.28cm/sec. depth 2 ft. 115°		4.79cm/sec. depth 8 ft.	3.65cm/sec. depth 10 ft.
Turbidity (Trans- mittance, %)	92½%			
Thermistor: Surface Temperature:	3110 ohms 30.9°C ½" from surface	3130 ohms 30.8°C 3 ¾" from surface		

REPRODUCIBILITY OF THE
ORIGINAL PAGE IS POOR

Remarks: K-3007 Thermistor, Unit #2, used for depth runs
K-805 Thermistor used for surface measurement

High Tide: 11:39 AM at Soldier Key

Low Tide: 6:12 PM at Soldier Key

TABLE 3-9

REMOTE SENSING DATA SHEET

Date 8/21/74

Location: B Lat. 25°41.00'
Long. 80°11.02'

Time: 10:50AM

Air Temperature: 30.3°C

Humidity: 70%

Wind Speed: 896 Ft. per min.

Sea State: Smooth - light chop

Wind Direction: 145°

Sky Condition: Clear day
10% low clouds
75% high clouds

Depth: 13½ ft.

Infrared Surface Temperature: 30.3°C

	Near Surface Depth: 1 ft.	1/3 Depth From Surface Depth: 4 ft.	2/3 Depth From Surface Depth: 8 ft.	Near Bottom Depth: 13 ft.
Thermistor Readings in ohms	3200 30.5°C	3200 30.5°C	3200 30.5°C	3200 30.5°C
Thermometer Reading	31.0°C			
Current cm/sec Current Dir.	6.77cm/sec. depth: 2 ft. 135°	5.31 cm/sec. depth: 6 ft.	5.30cm/sec depth: 10 ft.	
Turbidity (Trans- mittance, %)	90%	90%	90%	90%
Thermistor: Surface Temperature:	3130 ohms 30.8°C ½" from surface	3150 ohms 30.5°C 3 ¾" from surface		

REPRODUCTION OF THIS
ORIGINAL PAGE IS POOR

Remarks: K-3007 Thermistor, Unit #2, used for depth runs
K-805 Thermistor, Used for surface measurement

High Tide: 11:39 AM at Soldier Key
Low Tide: 6:12 PM at Soldier Key

TABLE 3-10

REMOTE SENSING DATA SHEET

Date 8/21/74

Station: C Lat. $25^{\circ}39.59'$
Long. $80^{\circ}11.20'$

Time: 12:55PM

Air Temperature: 30.6°C

Humidity: 61%

Wind Speed: 594 ft. per min.

Sea State: Smooth

Wind Direction: 135°

Sky Condition: High broken clouds
clear day

Depth: 15 ft.

Infrared Surface Temperature: 31.5°C

	Near Surface Depth: 6"	1/3 Depth From Surface Depth: 4 ft.	2/3 Depth From Surface Depth:	Near Bottom Depth:
Thermistor Readings in ohms	3120 31.2°C	3140 31.0°C		
Thermometer Reading	33°C			
Current cm/sec Current Dir.	9.90cm/sec depth: 2 ft. 135°	10.5cm/sec depth: 6 ft.	7.29 cm/sec. depth: 10 ft	
Turbidity (Trans- mittance, %)				
Thermistor: Surface Temperature:	3140 ohms 30.8°C $\frac{1}{2}$ " from surface	3140 ohms 30.8°C 3 $\frac{3}{4}$ " from surface		

REPRODUCIBILITY OF THE
ORIGINAL PAGE IS POOR

Remarks: Due to loss and subsequent recovery of thermistor assembly, full depth run was not made. Loss of anchor and other problems curtailed testing after this station.
K-3007 Thermistor used for depth run (Unit #2)
K-805 Thermistor used for surface measurement

High Tide: 11:39 AM at Soldier Key
Low Tide: 6:12 PM at Soldier Key

IV. REMOTE SENSING WATER SURFACE TEMPERATURE STUDY

A. Introduction

Water surface temperature remotely measured by infrared radiometers aboard satellites and aircraft will be used to provide information for mathematical model development. These data will be used for providing initial and boundary conditions of the model as well as for testing and evaluating the model. A flow chart for the remote sensing study is given in Figure 4-1.

Ultimately, it is hoped that satellites can provide the accurate, high-resolution water temperature data needed for model studies, monitoring thermal pollution such as hot water plumes, and possibly locating cold water sources such as springs on the continental shelf for use as heat sinks.

The use of boats or other surface-based measuring systems would be too costly and time consuming for obtaining the necessary data on the time and space scales desired. Aircraft can obtain the data on the time and space scales desired but the logistics and expense of routine measurements makes them less desirable than satellites.

The space resolution of thermal IR temperature measuring systems used in the present generation of satellites does not provide as much detail as is desired. However, the resolution of these thermal sensors is improving with each new generation of satellites so that optimum resolution should be available in the future. Clouds may blank satellite borne sensors from seeing the ocean surface on some occasions but the frequency of observations is still better than obtainable by other means for similar costs.

The Kennedy Space Center's NASA-6 aircraft with an IR Thermal Scanner and photographic equipment made a research data gathering flight on 29 July 1974, 0800-1300 EDT. Thermal IR data were acquired from the Air Force DMSP and NOAA-2 satellites during this time period. Also, ground truth data were gathered by boat along an E-W line across Biscayne Bay beneath the aircraft flight path on this occasion. The aircraft made twelve west to east runs at 1,500 ft. altitude along this path during the 5-hour period while water temperature data were taken by boat. The main purpose of this first joint aircraft and surfacecraft data gathering expedition was to correlate measurements and to calibrate the airborne IR thermal scanner against the sea surface measurements. Also, the satellite IR data are being correlated with these aircraft and surface measurements.

B. Air Force Satellite Data

The Air Force Defense Meteorological Satellite Program (DMSP), formerly DAPP, satellites are in polar orbit. These sun-synchronous satellites are approximately 450nm above the earth and have a period of 101 minutes. In the operational mode, two satellites provide imagery data every six hours over any spot on the globe (sunrise, sunset, local noon and midnight). This imagery includes the visual, near infrared and infrared spectral intervals over a 1600 to 1800 nm swath below the satellite. Real time data within the acquisition range, approximately a radius of 1500 miles of the receiving station, is provided to several tactical sites whereas the Air Force Global Weather Central (AFGWC) at Omaha, Nebraska, receives stored data of global coverage.

The present capability of the DMSP includes the following:

<u>DATA TYPE</u>	<u>SPECTRAL INTERVAL</u>	<u>RESOLUTION</u>
VHR Data	.4 to 1.1 μ	0.3nm resolution
WHR Data	8 to 13 μ	0.3nm resolution
HR Data	.4 to 1.1 μ	2.0nm resolution
(HR data has a low light capability that "sees" at night).		
IR Data	8 to 13 μ	2.0nm resolution

The Very High Resolution data (VHR) "sees" in the visible and near infrared. The product output is a positive transparency that can be received at 1:7,500,000 or 1:15,000,000 scale. Sensor altitude and attitude variations are compensated for and foreshortening at the edges is removed. Flexibility is further provided in that the data can be enhanced to bring out cloud/land and cloud/cloud significant contrasting features. The infrared products (WHR and IR) receive emitted thermal energy from 310°K to 210°K. Flexibility is provided to receive 1°K increments in gray shade steps from 2 to 16 or a 25°K span of temperatures can be divided into 16 gray shade steps. Electronic circuitry in the sensors converts the sensed thermal IR energy directly into equivalent black-body temperature, making temperature the directly displayed parameter within the limits indicated. The High Resolution (HR) data (.4 to 1.1 μ) can be processed day and night. Accurate nighttime gridding can be accomplished by using city light identification from this HR data. (Refs. 1,2)

The present generation of these satellites uses the 0.3-mi and 2.0-mi resolution lenses interchangeably. Normally the 0.3-mi lens is used to acquire WHR data on the 8-13 μ thermal IR channel only for the midnight pass. During daylight passes, the 0.3-mi lens is usually switched to the 0.4-1.1 μ visual wavelength channel and the 2-mi lens is used on the IR channel. In 1975, a 0.3-mi lens is to be available at all times on the

IR channel of a new series of these satellites. Presently, the 0.3-mi lens can be used for IR data during the daylight passes by special request.

A DMSP local readout and data processing van is scheduled for installation at Kennedy Air Force Station, Florida, in 1975. At the present time, DMSP thermal IR data are obtained from other readout stations through the STAFFMET Section, Detachment 11, 6 Weather Wing, Air Weather Service, Patrick AFB, Florida.

C. NOAA Satellite Data

The National Oceanic and Atmospheric Administration NOAA-2 and NOAA-3, ITOS series of satellites provide thermal IR data in the 10.5 to 12.5 micron region. This modified version of the Improved TIROS Operational Satellite (ITOS D-G) became operational in 1972. A Very High Resolution Radiometer (VHRR) with 9.5nm resolution provides the thermal IR data. These satellites are in sun-synchronous, 790 nm polar orbit with a period of 115.14 minutes. (Ref. 3)

The thermal IR data which we use from the NOAA-2 and NOAA-3 satellites is received at Wallops Island, Virginia, and processed at the National Environmental Satellite Services (NESS) facility in Suitland, Maryland. Data for the Florida area are available on southbound passes at approximately 0945 EDT (1345Z) and on northbound passes at 2100 EDT (0100Z). For minimum distortion and maximum resolution, it is desirable to have the satellite pass directly over our research area. The NOAA-2 and NOAA-3 orbits are not identical and both have a precession of about one degree of longitude per day in order to remain sun-synchronous. Therefore, the orbital track of one of these satellites is usually better than the other for our use on a given day.

These satellites also have a Vertical Temperature Profile Radiometer (VTPR) for obtaining atmospheric temperature and water vapor profiles by measuring spectral radiance in eight intervals in the infrared. Energy is measured in the 11 micron atmospheric window to deduce radiances free from effects of clouds in the other seven channels. Then six cloud free, discreet, narrow intervals in the 15 micron CO₂ region are measured to infer the atmospheric temperature profile. Finally, radiance in a single spectral interval near 18.7 microns in the rotational water vapor absorption band is measured and used to estimate water vapor concentrations in the troposphere. (Refs. 3, 4, 5, 7)

This VTPR system is presently used by NESS primarily to obtain temperature profiles and moisture data over the oceans or other places where no radiosonde balloon measurements are available. However, if needed, special computations can be made to obtain water vapor data for applying absorption corrections to our thermal IR measurements of sea surface temperature. In Florida, radiosonde data are normally available for this purpose.

D. NASA-6 Aircraft Flight

On 29 July 1974 the Kennedy Space Center NASA-6 Beechcraft C-45H made research flights over Biscayne Bay at Miami, Florida, while NOAA and Air Force satellites with thermal IR radiometers were passing overhead and a boat was gathering ground truth data in the Bay. The aircraft flew at 1500 ft. altitude and made twelve west to east data passes across Biscayne Bay between 0800 EDT (1200Z) and 1300 EDT (1700Z).

A race track course was flown with data collection starting over land near Cutler Ridge Power Plant and continuing to a channel marker buoy in the western part of the Bay thence eastward on approximately a 90-degree heading to Soldier Key on the east side of the Bay where each data run was terminated, see Figure 4-2.

No data were gathered on the westbound return flights which were made to the north of this course. Water temperature data were gathered by boat along the course from the channel marker buoy eastward to Soldier Key on this date.

The 8-14 micron IR Thermal Scanner was used to remotely sense the sea surface temperature from the aircraft. Its field of view is 2.5 milliradians and it scans through 77°20' degrees of arc normal to the flight path of the aircraft. It has an 18° F usable dynamic range and for our project it was calibrated to measure temperatures from 76°F to 94°F. The analog readout was recorded on magnetic tape aboard the aircraft. These data were later transferred from the tape to 70-mm film at Kennedy Space Center for our use. A calibration of the film gray scale density in terms of temperature was provided.

A 9" by 9" aerial camera was also used to take color photographs along the flight path on some data passes. This was to record positions of the boat and some key land marks in addition to possibly showing turbidity patterns in the Bay. The first six thermal IR data passes were flown between 0800 and 1000 EDT with color photography on the last pass. The last six data passes were flown between 1100 and 1300 EDT with color photography on the first and last passes.

E. Radiosonde Data for Water Vapor Corrections of IR Measurements

Rawinsonde balloons are launched daily at Miami International Airport and Kennedy Air Force Station at 0800 EDT (1200Z) and 2000 EDT (0000Z). They obtain pressure, temperature, humidity, wind speed, and wind direction data to altitudes in excess of 50,000 ft. Most of the atmospheric moisture is contained in the troposphere below 30,000 ft. Therefore, these soundings can be used to calculate the precipitable water that will attenuate our thermal IR measurements of sea surface temperature from aircraft or spacecraft on a given day.

Figure 4-3 is the Miami sounding for 0800 EDT on 29 July 1974 when the NASA-6 aircraft research flight was made over Biscayne Bay. The precipitable water content of the atmosphere was obtained by graphically determining the mean vapor pressure (e) in millibars of the atmospheric layers between plotted points on this sounding. The water content for each of these layers was then calculated using the equation:

$$W \text{ cm} = \frac{0.622}{g} e \ln P_2/P_1$$

where g is the acceleration of gravity, P_1 is the pressure at the top of the layer, and P_2 is the pressure at the bottom in millibars. The total W was then obtained by summing these values for all layers of the sounding.

Table 4-1 presents the precipitable water computed by layers for the 1200Z sounding, 29 July 1974. These data can be applied to the nomograms in Figure 4-4 to obtain the temperature corrections for the thermal IR sea surface temperatures measured from satellites. (Ref. 6) Since the atmosphere was extremely moist on this occasion, it is necessary to extrapolate the Kelvin temperature curves in Figure 4-4 up to the 5 cm precipitable water line. Table 4-4 also provides data for lower altitudes that can be used to apply corrections to IR temperature measurements made from aircraft.

F. Satellite Data and Results

On the morning of 29 July 1974, the NOAA-3 satellite pass was too far west of our research area for optimum use. Thermal IR photographs were obtained from the NOAA-2 satellite which passed east of Florida, Figure 4-5. South Florida is in the upper left hand corner of this photograph with Cuba shown near the center of the photograph.

Unfortunately, a trough of low pressure was along the east coast of Florida and it produced extensive clouds and rain. Our area of interest at approximately 25.5°N and 80.3°W is masked by a NE-SW band of clouds over the coastal area. The National Environmental Satellite Service in Washington is preparing an enlarged and enhanced thermal IR photograph of the Miami area in place of Figure 4-5. However, there is little hope of using it to measure sea surface temperatures in Biscayne Bay because of the cloud cover. The main objective is to develop satellite data processing techniques that can be applied to our future experiments. For our purposes, it is necessary to de-emphasize the clouds and enhance the gray scale to portray sea surface temperatures.

The Air Force DMSP satellite thermal IR data for 29 July 1974 has not been received. Enlarged photographic prints of the data are presently being made at Patrick Air Force Base, Florida. We have been informed that extensive cloud cover also existed at the times of the DMSP satellite passes and little or no usable data are available for Biscayne Bay.

Figure 4-6 is a DMSP satellite thermal IR photograph with one-degree Kelvin gray scale steps taken on 24 March 1972. This illustrates the capability of the DMSP and is typical of the quality of sea surface temperature data that can be obtained in the absence of clouds. The IR sensor on this satellite has 0.3-nmi resolution so that enlarged photographs can be used to produce greater detail in the area of interest.

It is improbable that future research data gathering flights on this project will encounter as much cloudiness over coastal waters in the forenoon as occurred on 29 July 1974. Certainly flights made during the South Florida dry season, November through May, should be better than this July case. Also, to increase the number of cases for study, thermal IR satellite

data will be acquired for days when only surface measurements are made by boat and no aircraft data are collected. Clouds will always be a problem on some occasions but if enough days are sampled some satellite passes are certain to produce cloud free results for a given location.

The main results of our satellite study have been to identify problems and limitations of the data and to develop, with the aid of the Air Force and the National Environmental Satellite Service, methods for enhancing and enlarging thermal IR displays for mesoscale sea surface temperature measurements. This is a pioneering effort in analysis on this small scale. We are pushing the state-of-the-art and are looking forward to the future development of spacecraft thermal IR sensors with better resolution than the 0.3 to 0.5 nautical mile available today. Up to this time, thermal IR sea surface temperature measurements from satellites have been used for macroscale studies over the broad oceans where one reading per degree of latitude and longitude was usually adequate.

Further research will be carried out on the 29 July 1974 experiment if usable satellite thermal IR sea surface temperature data can be produced. In that event, Table 4-1 and Figure 4-4 will be used to correct the IR measured sea surface temperatures for atmospheric water vapor absorption losses. Then the resulting corrected temperatures will be correlated with ground truth measurements taken by our boat in Biscayne Bay.

Some noise and calibration problems occurred with the thermal IR measurements from the NASA-6 aircraft on 29 July. Part of the data showing the Cutler Ridge Power Plant discharge plume of warm water and the area of Biscayne Bay near Soldier Key may be usable, if it can be calibrated, for correlation with the boat and satellite observations. Gray-shade steps for one-degree temperature increments are desired for the aircraft filmed IR data in order to match the temperature resolution of the boat measurements and take into account small temperature gradients in some parts of the Bay.

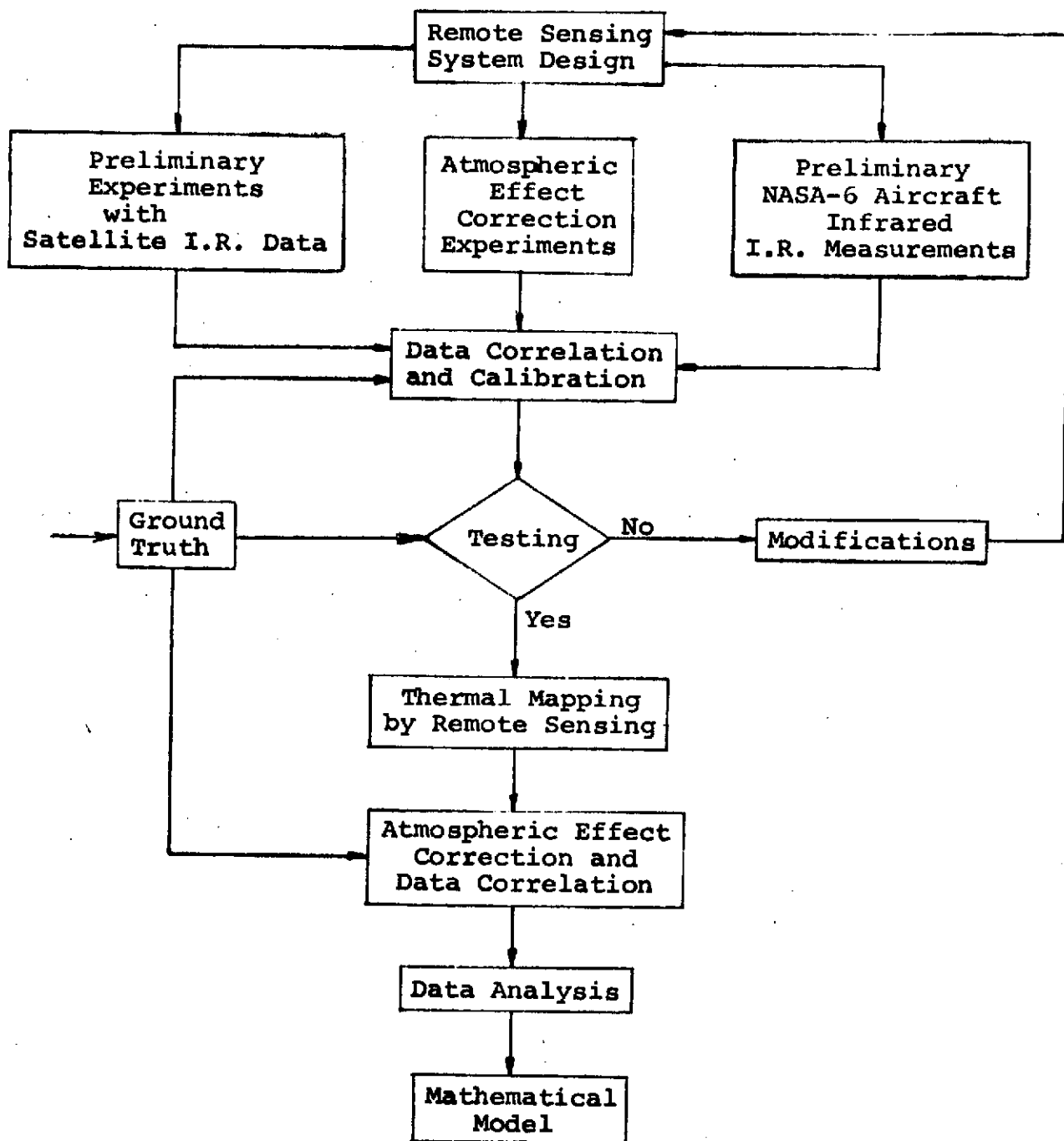


Fig. 4-1. Flow Chart for Remote Sensing Study

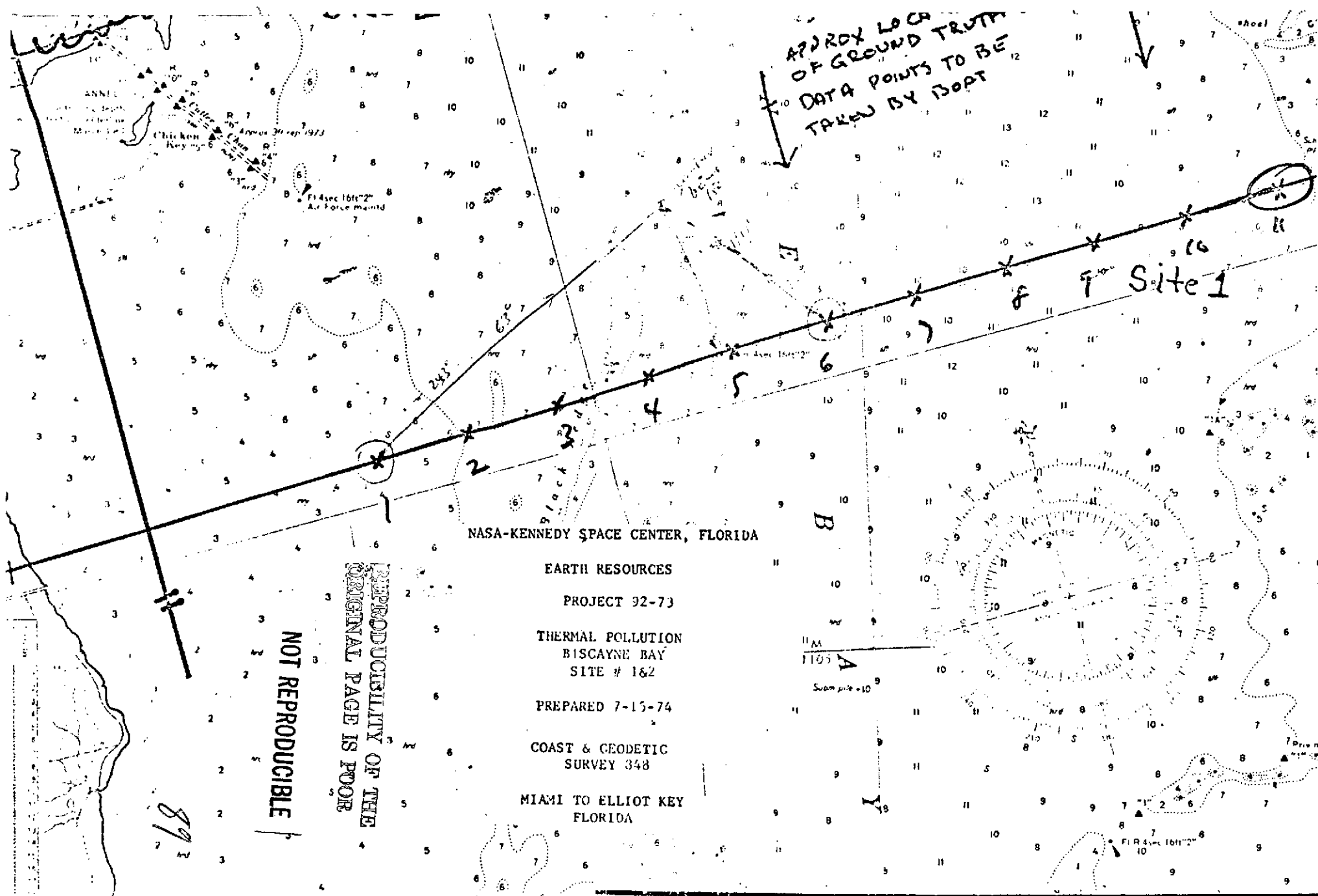
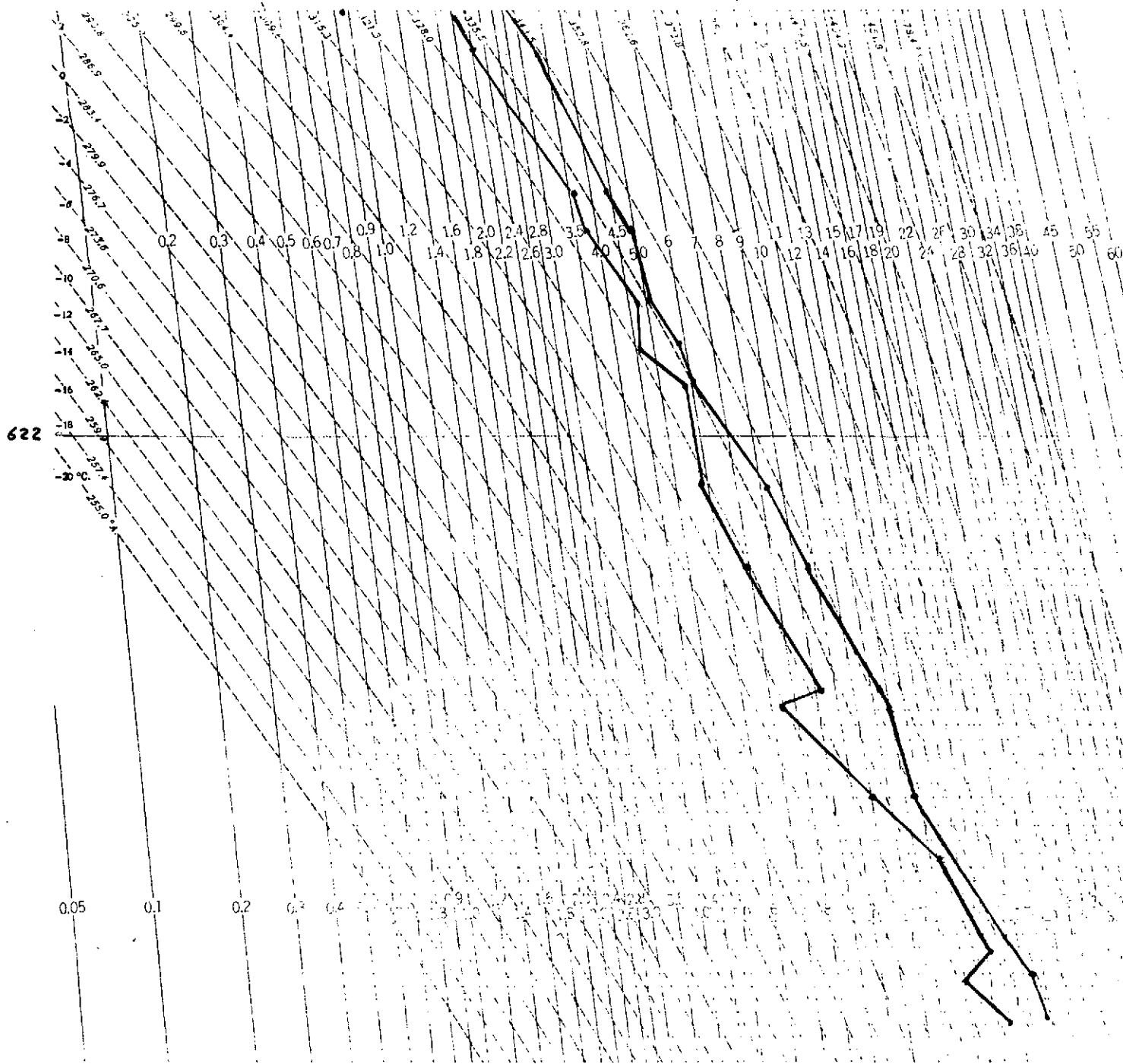


Fig. 4-2 Flight Path of NASA-6 Beechcraft



REPRODUCIBILITY OF THE
ORIGINAL PAGE IS POOR

-06-

Fig. 4-3. Miami Rawinsonde 1200Z, 29 July 1974

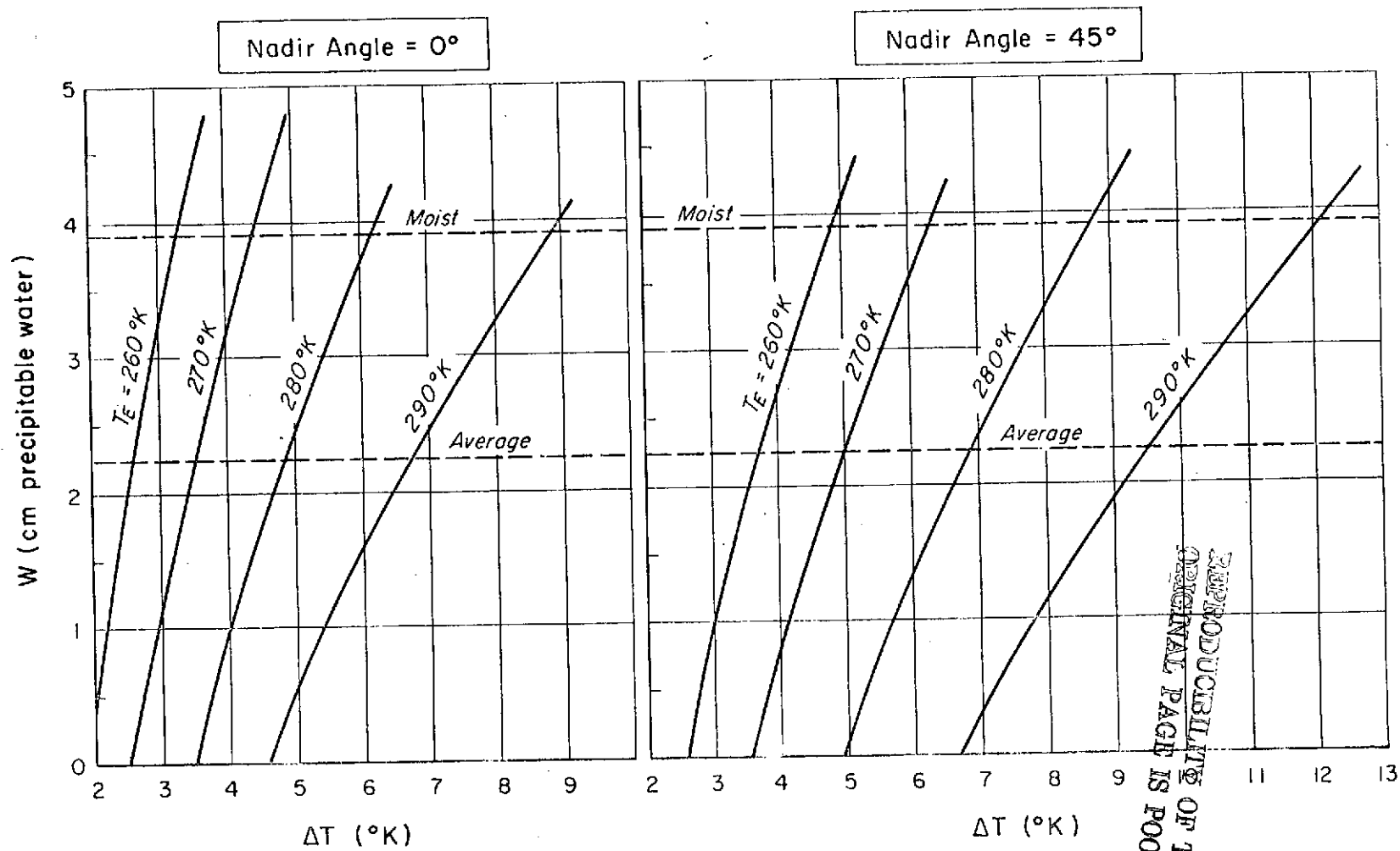
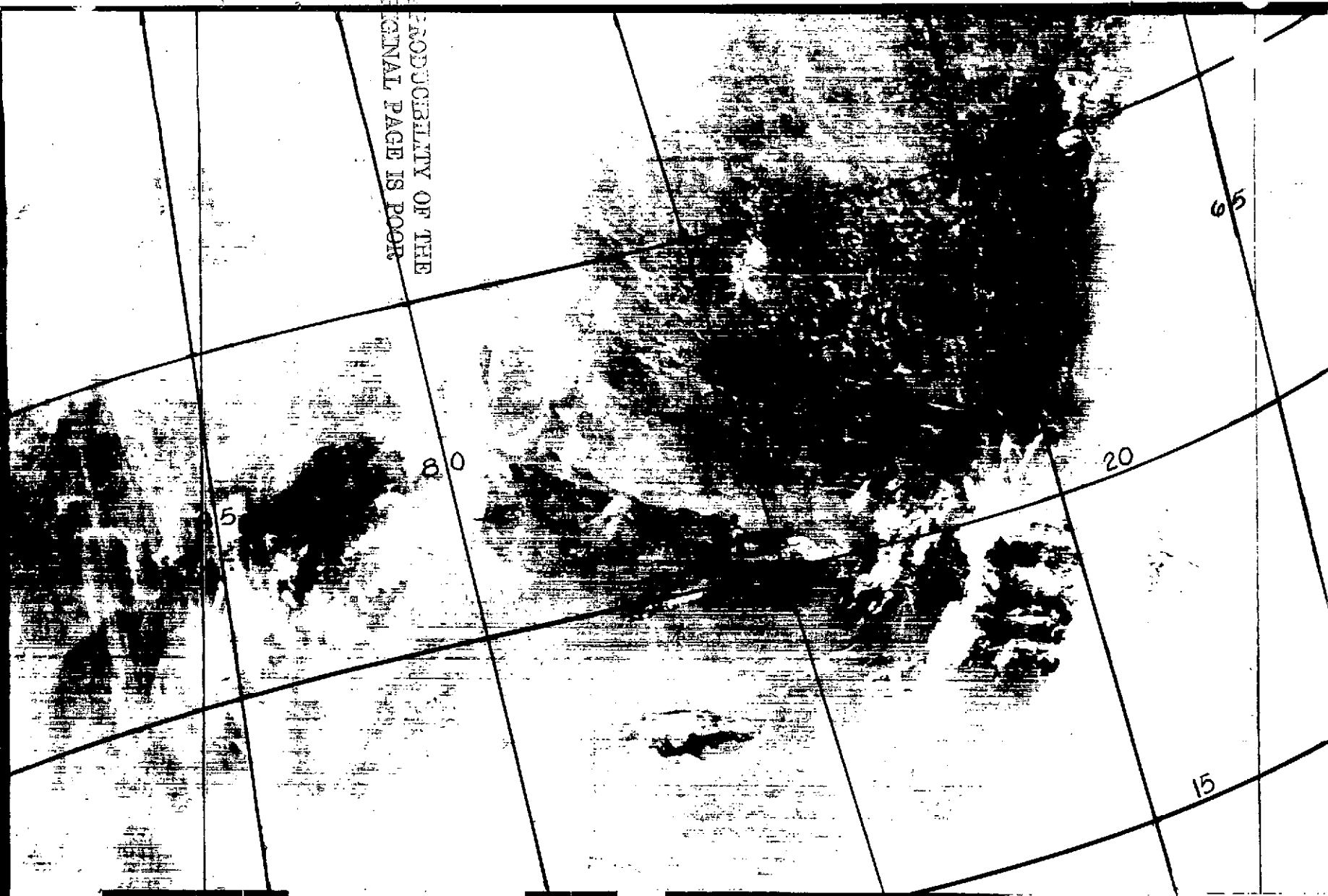


Fig 4-4 Clear-Sky Temperature Corrections

REPRODUCIBILITY OF THE
ORIGINAL PAGE IS POOR

REPRODUCIBILITY OF THE
ORIGINAL PAGE IS POOR



-92-

WAL 131:39:1:39 8162 I3F4451 VHRR MINCOM N-2

Fig. 4-5. NOAA-2 THERMAL IR PHOTOGRAPH, 1000 EDT (1400 Z) 29 July 1974

-93-

REPRODUCIBILITY OF THE
ORIGINAL PAGE IS POOR

294°



FIG. 4-6. THERMAL IR (8-13 μ) DATA FROM THE AIR FORCE DMSP SATELLITE EARLY ON MARCH 1972. (WHITE COLDER THAN 294°K, LIGHT GRAY 294-295°K, DARK GRAY 295-296°K BLACK WARMER THAN 296°K). 0.3 NM RESOLUTION

TABLE 4 -1. PRECIPITABLE WATER AT MIAMI, 1200 Z,
29 JULY 1974

Approximate Altitude Feet	Layers P_1/P_2	Mean e for Layer	Accumulative W cm for Layers
23,600	400	1.38	5.376
21,400	438		
	438	2.25	5.299
18,300	500		
	500	3.1	5.113
17,400	518		
	518	3.7	5.045
16,000	550		
	550	4.4	4.907
14,600	580		
	580	5.1	4.762
13,800	598		
	598	6.2	4.665
11,400	658		
	658	7.0	4.296
9,900	700		
	700	9.8	4.027
7,100	780		
	780	10.6	3.367
6,700	790		
	790	12.4	3.283
4,800	850		
	850	17.8	2.718
3,300	895		
	895	22.8	2.1479
2,000	940		
	940	29.0	1.4516
700	985		
	985	28.0	.6081
Surface	1020		

REFERENCE

1. STAFFMET Section, Detachment 11, 6 Weather Wing, Air Weather Service, DEFENSE METEOROLOGICAL SATELLITE PROGRAM (DMSP), Patrick Air Force Base, Florida, 1973.
2. Meyer, Walter D., "Data Acquisition and Processing Program: A Meteorological Data Source," BULLETIN OF THE AMERICAN METEOROLOGICAL SOCIETY, Volume 54, Number 12, December 1973.
3. Schwalt, A., MODIFIED VERSION OF THE IMPROVED TIROS OPERATIONAL SATELLITE (ITOS D-G), NOAA Technical Memorandum NESS 35, U.S. Department of Commerce, Washington, D.C., April 1972.
4. McMillin, L.M., Wark, D.Q., Siomkajlo, J.M., Abel, P.G., Werbowetzki, A., Lauritson, L.A., Pritchard, J.A., Crosby, D.S., Woolf, H.M., Luebke, R.C., Weinreb, M.P., Fleming, H.E., Bittner, F.E., Hayden, C.M., Satellite Infrared Soundings From NOAA Spacecraft, NOAA Technical Report NESS 65, U.S. Department of Commerce, Washington, D.C., September 1973.
5. Weinreb, Michael P. and Crosby, David S., Estimation of Atmospheric Moisture Profiles From Satellite Measurements by a Combination of Linear and Non-Linear Methods, National Environmental Satellite Service, NOAA, Washington, D.C., June, 1973.
6. Greaves, James R., Wexler, Raymond and Bowley, Clinton J., The Feasibility of Sea Surface Temperature Determination Using Satellite Infrared Data, NASA Contractor Report CR-474, Washington, D.C., May 1966.
7. Fritz, S., Wark, D.Q., Fleming, H.E., Smith, W.L., Jacobowitz, H., Hilleary, D.T., and Alishouse. Temperature Sounding From Satellites, NOAA Technical Report NESS 59, July 1972.
8. Ewing, G.C. (Edited by), Oceanography From Space, Ref. No. 65-10 Woods Hole Oceanographic Institution, Woods Hole, Massachusetts, 02543, April 1965.